

Leptoquark Searches at TeV Scale Using Neural Networks at Hadron Collider

Ijaz Ahmed,^{1,*} Usman Ahmad,^{2,†} Jamil Muhammad,^{3,‡} and Saba Shafaq^{4,§}

¹*Federal Urdu University of Arts, Science and Technology, Islamabad, Pakistan*

²*Riphah International University, Islamabad, Pakistan*

³*Sang-Ho College, & Department of Physics,
Konkuk University, Seoul 05029, South Korea*

⁴*International Islamic University, Islamabad, Pakistan*

(Dated: May 15, 2024)

Abstract

Several discrepancies in the decay of B-meson decay have drawn a lot of interest in the leptoquarks (LQ), making them an exciting discovery. The current research aims to discover the pair-production of leptoquarks that links strongly to the third generation of quarks and leptons at the center of mass energy $\sqrt{s}=14$ TeV, via proton-proton collisions at the Large Hadron Collider (LHC). Based on the lepton-quark coupling parameters and branching fractions, we separated our search into various benchmark points. The leading order (LO) signals and background processes are generated, while parton showering and hadronization is also performed to simulate the detector effects.

The Boosted Decision Trees (BDTs), Multilayer Perceptron (MLP), and Likelihood (LH) methods are effective in improving signal-background discrimination compared to traditional cut-based analysis. The results indicate that these machine learning methods can significantly enhance the sensitivity in probing for new physics signals, such as LQs, at two different integrated luminosities. Specifically, the use of BDTs, MLP, and LH has led to higher signal significances and improved signal efficiency in both hadronic and semi-leptonic decay modes. The results suggest that the LQ masses of 500 GeV and 2.0 TeV in fully hadronic decay modes can be accurately probed with signal significance 176.70 (17.6) and 184.27 (0.01) for MVA (cut-based) at 1000 fb^{-1} , respectively. Similarly, in semi-leptonic decay mode the signal significance values are 168.56 and 181.89 at lowest and highest selected LQ masses respectively for MVA method only. The enhanced numbers by a factor of 2 are also reported at 3000 fb^{-1} .

PACS numbers: 12.60.Fr, 14.80.Fd

Keywords: Leptoquarks, Collider, Coupling, Significance, MC Event Generator.

*Electronic address: ijaz.ahmed@fuuast.edu.pk

†Electronic address: usmanahmed1661@gmail.com

‡Electronic address: mjamil@konkuk.ac.kr

§Electronic address: saba.shafaq@iiu.edu.pk

I. INTRODUCTION

So far, the precision with which the Standard Model (SM) predictions have been confirmed is astonishing. However, certain enduring discrepancies in rare B-meson decays discovered across multiple distinct investigations suggest the existence of novel physics. For instance, the BaBar collaboration revealed an important surplus in the R_D^* observables for the first time in 2012 [1, 2]. Among the several extensions of SM simplest one is a scenario involving a tree-level exchange of Leptoquarks (LQs). These are the particles that may convert a lepton into a quark and vice versa, and establish a link between the lepton and quarks sectors in the SM [3–9], which have comparable structures.

Color-triplet bosons that possess both lepton and baryon numbers are known as leptoquarks. Other quantum numbers are (fractional) electric charges having spins 0 (scalar LQ or "sLQ") or 1 (vector LQ or "vLQ") depending upon the model under consideration. They do not exist in ordinary matter and, like the majority of other elementary particles, only survive for relatively brief periods. Also, they must carry color charge making them possible to interact with gluons. In general, a leptoquark may interact with any combination of a quark and lepton with given electric charges (which yields up to $3 \times 3 = 9$ definite interactions of a single type of LQ).

Various searches for LQs coupling to the first, second, and third generations have been published by ATLAS and CMS [10–14]. With distinct electric charges, each generation of leptoquarks is divided into up-type and down-type LQs. They are divided, for example, into down-type LQs (LQ_3^d), which decay into $t\tau$ or $b\nu$, and up-type LQs (LQ_3^u), which decay into $b\tau$ or $t\nu$ for the third generation. The LHC phenomenology of a scalar leptoquark with quantum numbers under the SM gauge group $S_1 = (\bar{3}, 1, 1/3)$ has been examined in this article. The leptoquark's existence also substantially improves the electroweak vacuum's stability [15]. Limits on the parameters of the various leptoquark model aspects are derived under the assumption of various branching fractions. A recent study at 13 TeV data from CMS collaboration puts a bound on scalar LQ of mass ≥ 900 GeV in the search through $t\tau$ final states with 100% branching fraction [16]. The ATLAS Collaboration performed a cut-based analysis in a recent study [17] and derived the limit for the up-type third-generation scalar leptoquark, presuming that LQ decays to a top quark as well as neutrino with a branching ratio of 100%. The leptoquark to $t\tau$ decays will be preferred over other decay modes by the third generation. Check out references [18, 19] for the most current constraints

on the vector leptoquark from collider searches.

$(SU(3), SU(2), U(1))$	Spin	Symbol	Type	F
$(\bar{3}, 3, 1/3)$	0	S_3	$LL(S_1^L)$	-2
$(3, 2, 7/6)$	0	R_2	$RL(S_{1/2}^L), LR(S_{1/2}^R)$	0
$(3, 2, 1/6)$	0	\tilde{R}_2	$RL(\tilde{S}_{1/2}^L), \overline{LR}\tilde{S}_{1/2}^L$	0
$(\bar{3}, 1, 4/3)$	0	\tilde{S}_1	$RR(\tilde{S}_0^R)$	-2
$(\bar{3}, 1, 1/3)$	0	S_1	$LL(S_0^L), RR(S_0^R), \overline{RR}(S_0^R)$	-2
$(\bar{3}, 1, -2/3)$	0	\tilde{S}_1	$\overline{RR}(\tilde{S}_0^R)$	-2

TABLE I: List of Scalar Leptoquarks

A. LQ Model $S_1 = (\bar{3}, 1, 1/3)$

Five possible operators that represents the interaction of S_1 with fermions are;

$$\begin{aligned} \mathcal{L} \supset & +y_{1\ ij}^{LL} \bar{Q}_L^C{}^{i,a} S_1 \epsilon^{ab} L_L^{j,b} + y_{1\ ij}^{RR} \bar{u}_R^C{}^i S_1 e_R^j + y_{1\ ij}^{RR} \bar{d}_R^C{}^i S_1 \nu_R^j \\ & + z_{1\ ij}^{LL} \bar{Q}_L^C{}^{i,a} S_1^* \epsilon^{ab} Q_L^{j,b} + z_{1\ ij}^{RR} \bar{u}_R^C{}^i S_1^* d_R^j + h.c. \end{aligned} \quad (1)$$

Whereas τ^κ having $\kappa = 1, 2, 3$, are Pauli matrices $i, j = 1, 2, 3$ ($a, b = 1, 2$) are flavor $SU(2)$ indices, $\epsilon^{ab} = (\tau^2)^{ab}$ and the superscript C stands for charge conjugation operator. An arbitrary complex $3 \otimes 3$ Yukawa coupling matrix has the entries $y_{1\ ij}^{LL}$. In contrast, the $z_{1\ ij}^{LL}$ matrix is antisymmetric in flavor space, i.e., $z_{1\ ij}^{LL} = -z_{1\ ji}^{LL}$. In terms of quark-lepton and quark-quark pairings, the matrices y and z represent the strength of the LQ interaction. When the LQs only couple to left- or right-chiral quarks, respectively, they are referred to as left- and right-type LQs [20]. In flavor space, $z_{1\ ij}^{LL}$ is a symmetric matrix (i.e $z_{1\ ij}^{LL} = z_{1\ ji}^{LL}$) [21] while all other matrices are hypothetical and entirely arbitrary.

The R_D^* anomalies may be well explained by LQs (often S_1) that pair to these fermions. Also, it helps us to understand the anomalous magnetic moment of muon [22].

Total decay widths of leptoquarks result in a pair of leptons and quarks [23]

$$\Gamma_{j=0} = \sum_i \frac{\lambda_i^2}{16\pi} M_{LQ} \quad (2)$$

where j here indicates the spin of the leptoquark, and the sum is extended to all possible decay modes of the leptoquark. The above equation shows the total decay width for scalar leptoquarks. We have to calculate partial decay width,

for this, we have to divide partial decay width by total decay width as shown in 1Total decay width vs lambda for third generation sLQ at different massesfigure.1.

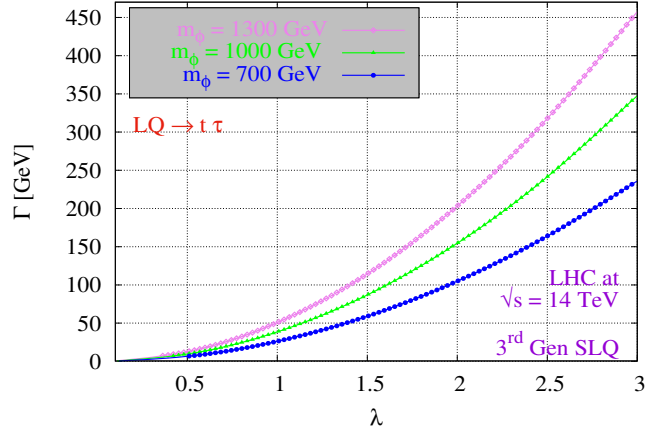


FIG. 1: Total decay width vs lambda for third generation sLQ at different masses.

All particles, including leptoquarks, tend to decay wider overall as their mass increases. Higher mass particles may be permitted to exist in a wider range of energy states, which might result in a wider variety of decay modes and a wider overall decay breadth. This indicates that there are often more decay channels available for heavier particles. A wider decay width results from an increase in the number of available decay channels caused by an increase in the coupling between a leptoquark and other particles. This increases the chance of decay and, thus, the decay width of the leptoquark since it can decay into a greater range of particles. Fig.2Production cross-section vs lambda for 3rd Gen sLQ at different masses of LQfigure.2

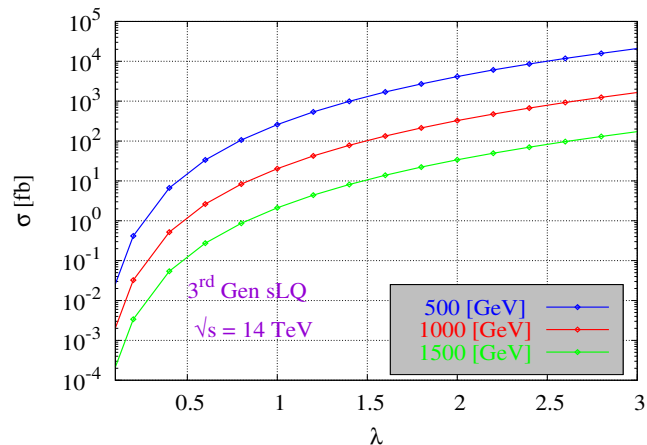


FIG. 2: Production cross-section vs lambda for 3rd Gen sLQ at different masses of LQ.

describes the relationship between λ vs σ for third-generation scalar leptoquark. As the coupling

strength directly affects the probability of the leptoquark interacting with other particles, increasing it causes the cross-section to rise as well. A bigger cross-section in particle collisions indicates the probability of a certain interaction happening, and a higher coupling strength indicates that the leptoquark will interact with other particles more frequently.

II. BENCHMARK POINTS

The searches for the ultimate states resulting from combinations of leptoquark decays to the third (t τ) generations are the main topic of this article. We choose three benchmark points based on such decays, which are listed in Table IIBenchmark scenarios for third generation scalar LQ_s table.2.

BP's	Scalar Leptoquark	m_ϕ [GeV]	λ_{33}
BP1	Third Generation	(500,...2000)	0.5
BP2	Third Generation	(500,...2000)	1.0
BP3	Third Generation	(500,...2000)	1.5

TABLE II: Benchmark scenarios for third generation scalar LQ_s

III. PRODUCTION CROSS-SECTION

The parton-level leading order (LO) cross sections are provided by [24] for a scalar leptoquark.

$$\begin{aligned}\hat{\sigma}_{gg}^{LO} &= \frac{\alpha_s^2 \pi}{96 \hat{s}} \times [\beta(41 - 31\beta^2) + (18\beta^2 - \beta^4 - 17) \log \frac{1 + \beta}{1 - \beta}] \\ \hat{\sigma}_{q\bar{q}}^{LO} &= \frac{2\alpha_s^2 \pi}{27 \hat{s}} \beta^3 \\ \hat{\sigma}_{eq}^{LO} &= \frac{\pi \lambda^2}{4} \delta(\hat{s} - M_{LQ}^2)\end{aligned}$$

Here, the parton subprocess's invariant energy is represented by \hat{s} , and $\beta = \sqrt{1 - 4M_{LQ}^2/\hat{s}}$. The leptoquark pair-production cross-section is known to be essentially independent of the Yukawa couplings except for extremely high values.

The production cross-section of a pair-produced leptoquark in femto barn (fb) with the leptoquark mass fluctuation at the 14 TeV LHC is displayed in Figure 3Mass vs cross-section for third generation pair production sLQ at different values of lambda'sfigure.3. The phase space that may be used to produce leptoquarks gets smaller as their mass rises. Because

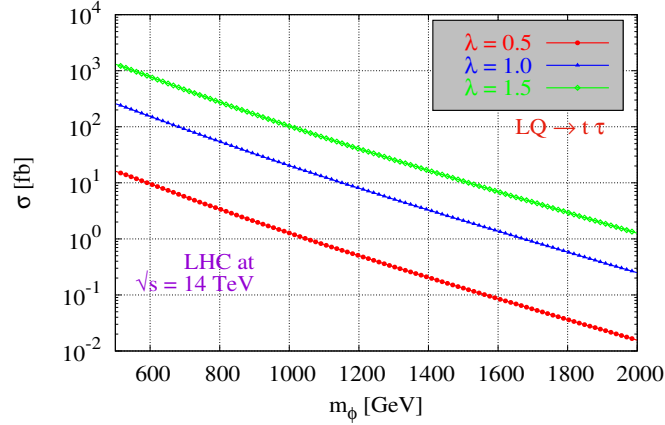


FIG. 3: Mass vs cross-section for third generation pair production sLQ at different values of lambda's.

of this, there is a lower chance of creating the leptoquark in high-energy collisions. With increasing mass, the leptoquark's coupling strength to the particles involved in its synthesis may diminish. The likelihood of producing the leptoquark in collisions is decreased by this lower connection. The production of the leptoquark becomes difficult at greater masses because of the more severe energy and momentum limits in the collision.

Leptoquark synthesis could become kinematically feasible at greater en-

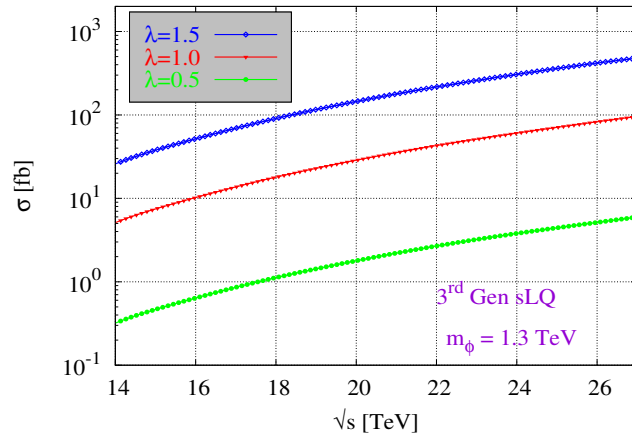


FIG. 4: Energy vs cross-section for third generation pair-production sLQ at different values of lambda's.

ergies. Accordingly, it is more likely for the particles to have sufficient energy to generate leptoquarks when the level of energy rises. Fig.4 Energy vs cross-section for third generation pair-production sLQ at different values of lambda's figure.4

shows the relationship between energy vs cross-section at different couplings. In particle collisions involving leptoquarks, the cross-section grows as the center of mass energy increases. Via exchanging kinetic energy, heavier particles may be created at a higher center of mass energies. This leads to a greater cross-section by increasing the number of alternative end states. More phase space is available for particle generation at higher energies. This increases the frequency of interactions and, consequently, the cross-section since there are more possibilities for the particles involved in the collision to organize themselves. Specific particle resonant generation is more likely at higher energies. The cross-section will grow as the energy gets closer to the resonance energy if the leptoquark manufacturing process is connected to any resonant states. Integrated luminosity is calculated as;

$$N = \sigma \int L dt = \sigma L_{int}, \quad (3)$$

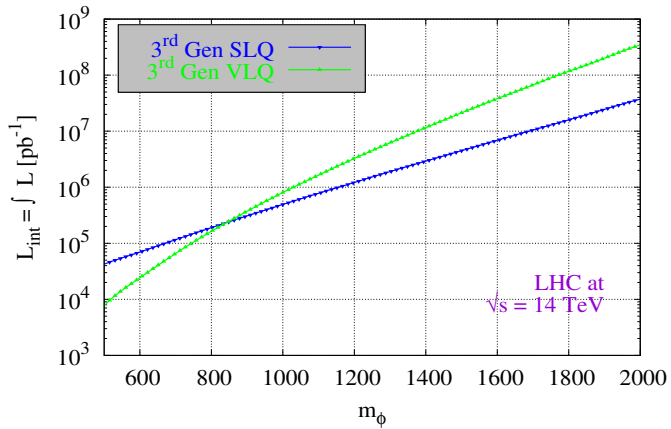


FIG. 5: Required integrated luminosity for 5σ .

IV. KINEMATICAL ANALYSIS

In this section, we present a kinematical analysis of leptoquarks production decay modes via calculations on invariant mass spectra, transverse momenta, pseudorapidity, and signal efficiency. Generation of signals and background events MadGraph v3.4.5 is used in this study to calculate cross-sections (σ). Similarly, events for both the signal and the background are generated using MadGraph v3.4.5, and these events are then written to an LHE file and compiled using PYTHIA v3.4.5. Additionally, PYTHIA determines their relative efficiency. The result is subsequently assessed using ROOT v6.26.02. Histograms and graphs are generated as well using ROOT.

Different scattering processes are employed as signals in the present research. The LHC p-p collisions at $\sqrt{s} = 14 \text{ TeV}$ produce all of these scattering modes. However, protons also include charged leptons because of quantum fluctuations, making it feasible to analyze lepton-driven events in the LHC. The collision of a lepton (ℓ) from one proton and a quark (q) from the other proton results in the resonant generation of an exotic leptoquark (LQ) state, which is the most basic example of this type of mechanism. In signal processes the following final states are possible for third-generation scalar leptoquark:

$$pp \rightarrow \phi\bar{\phi}, \phi \rightarrow t\tau, \phi \rightarrow \bar{t}\bar{\tau}, t \rightarrow bjj, \bar{t} \rightarrow \bar{b}\bar{jj} \quad (4)$$

$$pp \rightarrow \phi\bar{\phi}, \phi \rightarrow t\tau, \phi \rightarrow \bar{t}\bar{\tau}, \quad (5)$$

While evaluating these signal circumstances, we took into account the following SM background processes with comparable end-state topologies.

$$\begin{aligned} pp &\rightarrow t\tilde{t}z, (t \rightarrow bW^\pm, W^\pm \rightarrow l + vl), (\tilde{t} \rightarrow \tilde{b}W^\pm, W^\pm \rightarrow l\nu_{\tilde{l}}), (z \rightarrow jj) \\ pp &\rightarrow t\tilde{t}, (t \rightarrow bW^\pm, W^\pm \rightarrow l + vl), (\tilde{t} \rightarrow \tilde{b}W^\pm, W^\pm \rightarrow l - vl) \\ pp &\rightarrow t\tilde{t}w^\pm, t \rightarrow bw^+, w^+ \rightarrow l^+vl, \tilde{t} \rightarrow \tilde{b}w^-, w^- \rightarrow l - \nu_{\tilde{l}}, w^\pm \rightarrow jj \\ pp &\rightarrow t\tilde{t}, (t \rightarrow bjj), (\tilde{t} \rightarrow \tilde{b}\bar{jj}) \end{aligned} \quad (6)$$

The selection cuts applied are:

- Transverse momentum of the jet $p_T^j \geq 30 \text{ GeV}$.
- Lepton (e, μ, τ) are selected with $p_T^{lep} > 20 \text{ GeV}$.
- Absolute pseudorapidity for $|\eta^j| < 2.4$.
- Absolute pseudorapidity for $|\eta^{lep}| < 1.5$

The initial observations in high energy physics experiments are transverse momentum distributions of particles of final state. Statistical techniques have been frequently used in recent years to explain such multi-particle systems. A particle's transverse momentum can be described as:

$$P_T = \sqrt{P_{x^2} + P_{y^2}} \quad (7)$$

where the momentum variables in the transverse momentum axis are P_x and P_y . In terms of transverse energy, it is defined as:

$$E_T = \sqrt{M^2 + P_T^2} \quad (8)$$

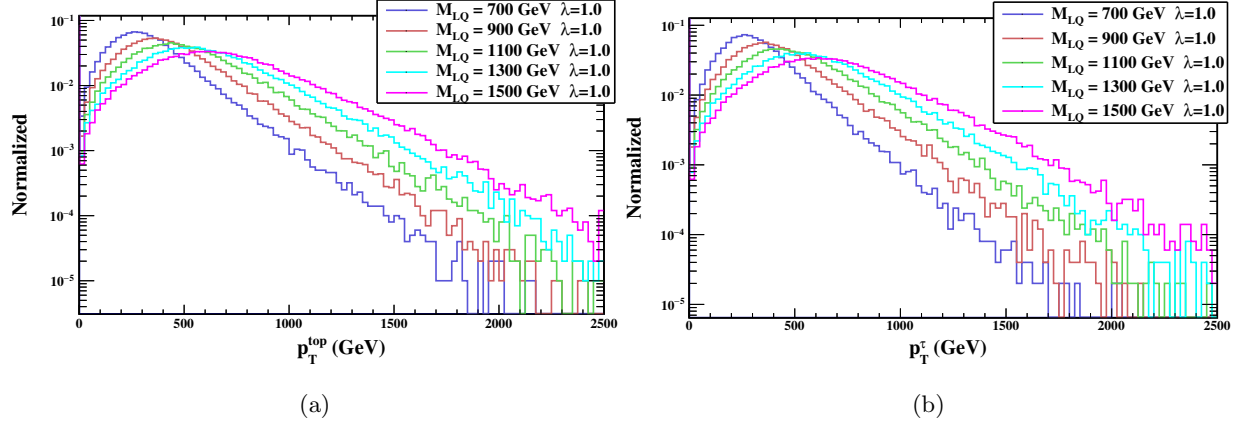


FIG. 6: Transverse momentum of top quark on left while transverse momentum of tau τ on right respectively.

Pseudorapidity is characterized by

$$y = \frac{1}{2} \ln \left(\frac{E + p_z}{E - p_z} \right) = \frac{1}{2} \ln \frac{1 + \cos \theta}{1 - \cos \theta} = \ln \cot \frac{\theta}{2} = \eta \quad (9)$$

Where η is the pseudorapidity. The term "pseudorapidity" is used to define the angle that a particle has concerning the beam axis. The beam axis is parallel to particles with $\eta = 0$, whereas particles with larger values are lost. To enhance the simulation findings on certain kinematical

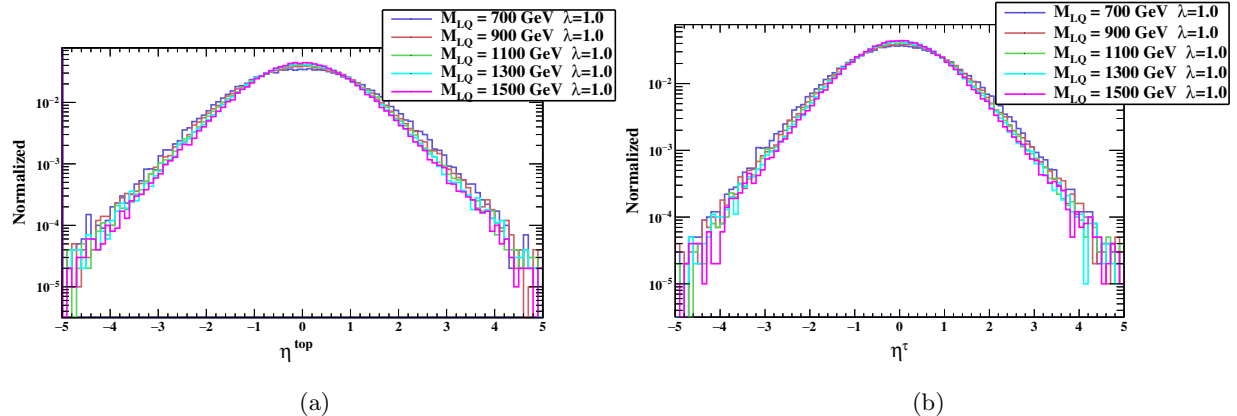


FIG. 7: Pseudorapidity of top quark on left while for τ on right respectively.

cuts in this work, 50000 events are created and integrated for signal processing. For jets, we select the cuts $p_T^j > 30 \text{ GeV}$. The center of mass energy $\sqrt{s} = 14 \text{ TeV}$ is used to determine each efficiency. Integrated luminosity 1000 fb^{-1} and 3000 fb^{-1} is used to calculate signal prominence. Using the momenta and energies of its decay products, the invariant mass of a leptoquark is a basic feature that measures the overall mass energy of the leptoquark system. Invariant mass is

an essential tool for understanding the characteristics and interactions of leptoquarks in particle physics studies as it is constantly independent of the observer's frame of reference.

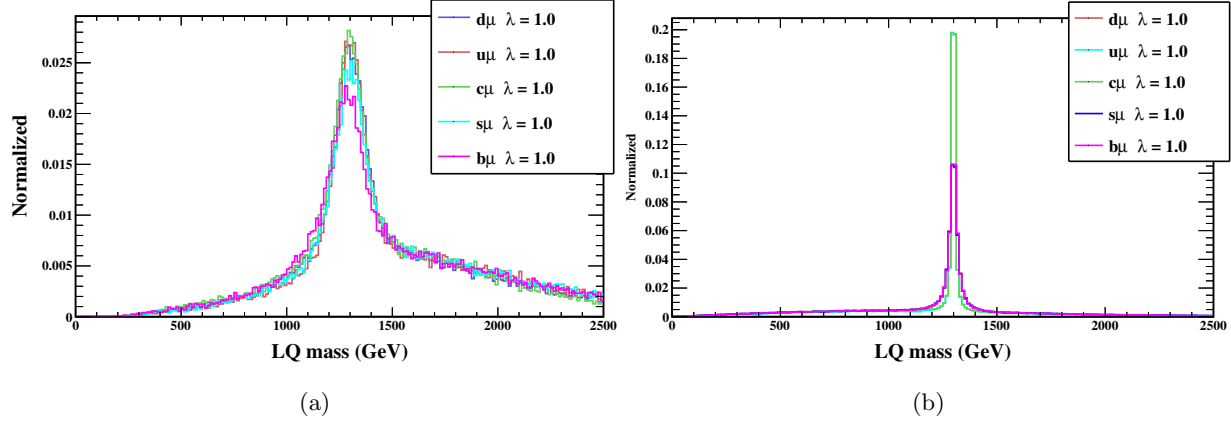


FIG. 8: Invariant mass of leptoquark for different quark flavour at $\sqrt{s} = 14 \text{ TeV}$.

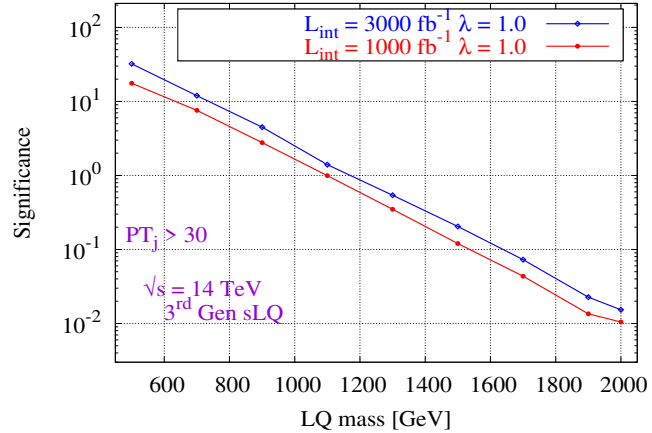


FIG. 9: Mass vs significance of P_T^j by considering 3^{rd} Gen sLQ (hadronic decay mode) at two different int. luminosity.

Fig.9 Mass vs significance of P_T^j by considering 3^{rd} Gen sLQ (hadronic decay mode) at two different int. luminosities. The plot represents mass vs significance at two different luminosity for third-generation scalar leptoquarks while considering its hadronic decay mode at $\sqrt{s} = 14 \text{ TeV}$. As we can see from Fig.9 Mass vs significance of P_T^j by considering 3^{rd} Gen sLQ (hadronic decay mode) at two different int. luminosities. With increasing mass of leptoquark the significance decreases accordingly. Such that at 500 GeV and 1000 fb^{-1} the significance is 17.59 and for 2 TeV the significance drops to 0.010. That might be due to the phase space that is open to the decay products of the leptoquark decreases as its mass rises. As a result, there are less accessible decay channels, which lowers the amount of

events that could be noticed. While at higher luminosity (3000fb^{-1}) and 500 GeV the value of significance increases up to 32.18. Similarly for 2 TeV, the value of significance becomes 0.015. A higher integrated luminosity causes the detector to record more collisions. The statistical significance of the detected signal over background fluctuations improved as a result of the larger number of signal occurrences caused by the enhanced statistics. Greater integrated luminosity provides more information to precisely estimate and minimize background contributions. Better background removal methods are made possible as a result, producing a more efficient signal and greater significance. Also, the experiment's sensitivity to rare phenomena, including the creation and decay of the third-generation scalar leptoquark, is increased by integrated luminosity. This increases the relevance by allowing signal events that were previously hidden by background noise to be detected.

V. MULTIVARIATE ANALYSIS

The "Toolkit for Multivariate Analysis" (TMVA), a ROOT-integrated framework, allows for the processing and calculation of many multivariate classification algorithms in simultaneously [25]. The classification has been performed considering two types of events: signal and background. TMVA is specially developed for applications of HEP nevertheless, it shouldn't bound for this only [26]. To provide an objective performance comparison of classifiers, TMVA runs in transparent factory mode[26] such as Optimization of the Rectangular Cut, the PDE Technique to Projective Likelihood Estimation, Multidimensional Probability Density Estimation, Boosted/Bagged Decision Trees, Support Vector Machine, Multilayer Perceptron. The data are presented with an abundance of auxiliary information, including the correlation matrix, parameter ranking, separation power, and, in final form, a complete efficiency vs background rejection curve of the trained classifiers.

A. Methods Used

We are representing three classifiers in our work; BDTs (Boosted Decision Trees), Likelihood, and Multilayer Perceptron (MLP). A detailed description of these classifiers is described below.

B. BDTs (Boosted Decision Trees)

A classification tool with a tree-like topology is called a decision tree. Repetitive left/right (yes/no) selections are made per every single test event, one variable at a time until the event reaches a node known as the "leaf node," which categorizes it as either background or signal. The phase space is separated into several distinct areas by the collection of leaf nodes, which are categorized as either signal or background type.

A modification of a single decision tree is represented by boosted decision trees. Individual decision tree classifications are integrated to create an ensemble of decision trees, and the classifier is determined by a (weighted) majority vote of each of the decision tree classifications.

C. Likelihood Ratio

Constructing an algorithm of one-dimensional probability density functions (PDFs) from the training data which replicates the data parameters for signal and background is the foundation for the maximum likelihood categorization method. By multiplying the signal probability densities of each input variable and normalizing the result by the total of the signal and background likelihoods, one may determine the likelihood that a particular occurrence corresponds to a given signal format. The probability ratio $y_L(j)$ for occurrence j is determined by

$$y_L(j) = \frac{L_S(j)}{L_S(j) + L_B(j)} \quad (10)$$

In addition, the following equation could be used to determine a candidate's likelihood of being signal or background:

$$L_{S/B}(j) = \prod_{i=1}^{n_{var}} P_{S/B,i}(x_i(j)) \quad (11)$$

while the probability density function for the i th input variable, x_i , is represented by $P_{S/B,i}$. To every i , the probability density function gets normalized at one:

$$\int_{-\infty}^{\infty} P_{S/B,i}(x_i) dx_i = 1 \quad (12)$$

D. Multilayer Perceptron

An architecture known as a Multilayer Perceptron, or neural network, is made up of many hidden layers of neurons, with each layer's output serving as the input for the subsequent layer's

neurons, as seen in Fig.10Layout of Neural networkfigure.10. The recurrent neural networks are examples of additional linkages that allow a neuron's output could be utilized as another neuron's input within a single layer. A binary classification tool or a multi-class classifier can be used to separate the signal of the noise [27].

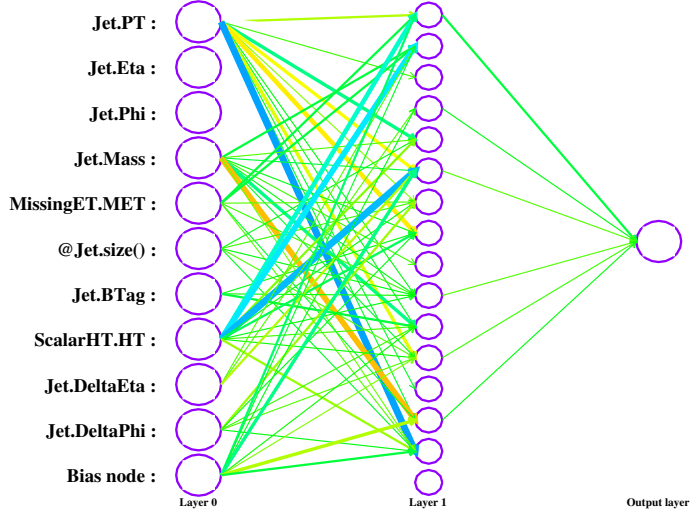


FIG. 10: Layout of Neural network

E. Signal Efficiency versus Background Rejection

The curve of background rejection against signal efficiency can be a useful tool for accurately estimating a classifier's performance. A high background rejection and a high signal efficiency are required to achieve the greatest separation of noise from signal candidates. The expected separation power of a classifier improves with increasing area. As we can see from Table IIIArea Under the Curve for 3rd Gen LQs with cuts values for both of the decay mode

3 rd Gen	LQs	MLP
---------------------	-----	-----

table.3 the best classifier which has greater **AUC** for 3rd Gen generation sLQ is **MLP**. For both hadronic and semi-leptonic decay modes, the **ROC** curves are shown in Fig.11Background rejection Vs signal efficiency for fully hadronic on the left and semi-leptonic on the right respectively. As we can see from Fig.11Background rejection Vs signal efficiency for fully hadronic on the left and semi-leptonic on the right respectively, the **MLP** classifier shows the highest value of **AUC** for both decay modes, which implies that the MLP classifier is very appropriate for this particular classification problem. For instance, in the case of fully hadronic mode, this gives a value of 0.914, similar behavior can be seen in semi-leptonic mode with a value of 0.896 (by applying cuts). This may indicate that the design and training procedure of the MLP is successfully identifying the important character-

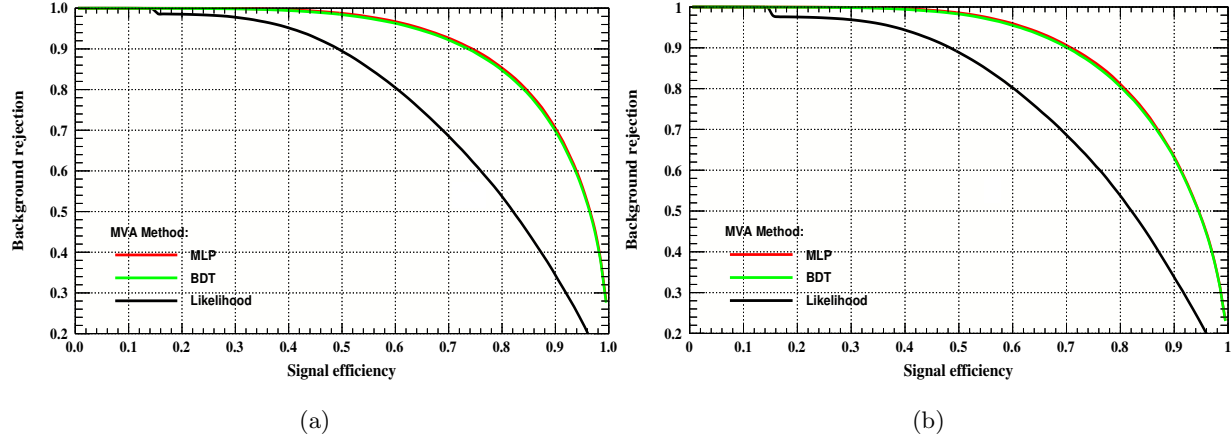


FIG. 11: Background rejection Vs signal efficiency for fully hadronic on the left and semi-leptonic on the right respectively (with cuts).

istics and patterns in the data associated with the Leptoquark signal. It may also suggest that the MLP classifier is more resilient and broadly applicable to various datasets and situations about third-generation scalar Leptoquark detection applications. Other classifiers (BDT and Likelihood) are showing prominent results with applying cuts as shown in Table IIIArea Under the Curve for 3rd Gen LQs with cuts values for both of the decay modetable.3. This suggests that they can separate the positive and negative occurrences to a great degree by capturing the minute variations and patterns unique to the Leptoquark particles. Reaching maximum AUC values indicates that the MLP, BDT, and Likelihood models are resilient to dataset variability and noise. They are less susceptible to be affected by random fluctuations or outliers and are capable of generalizing well to data that has not yet been observed.

MVA Classifier	AUC (hadronic)	AUC (semi-leptonic)
MLP	0.914	0.896
BDT	0.910	0.893
Likelihood	0.774	0.771

TABLE III: Area Under the Curve for 3rd Gen LQs with cuts values for both of the decay mode.

VI. CUT EFFICIENCY OF TMVA METHODS

Each classifier is trained for 50000 signal events and 50000 for background events. To check the total visibility of the signal process, signal significance is calculated for each classifier.

$$pp \rightarrow \phi\bar{\phi}, \phi \rightarrow t\tau, \phi \rightarrow \bar{t}\bar{\tau}, t \rightarrow bjj, \bar{t} \rightarrow \bar{b}jj \quad (13)$$

$$pp \rightarrow \phi\bar{\phi}, \phi \rightarrow t\tau, \phi \rightarrow \bar{t}\bar{\tau}, t \rightarrow bw^+, w^+ \rightarrow l^+\nu l, \bar{t} \rightarrow \bar{b}, w^-, w^- \rightarrow l^-\bar{\nu}l \quad (14)$$

Eq.13equation.6.13 represents a third-generation scalar leptoquark for fully hadronic decay, having two top quarks, two tau leptons, two b-jets, and four light jets in the final states. Signal significance is calculated by using cuts as follows;

$$P_T^{jet} > 30GeV, Jet_{size} \geq 8, |\eta_{jet}| < 2.5$$

$$P_T^{jet} > 30GeV, Jet_{size} \geq 6, |\eta_{jet}| < 2.5$$

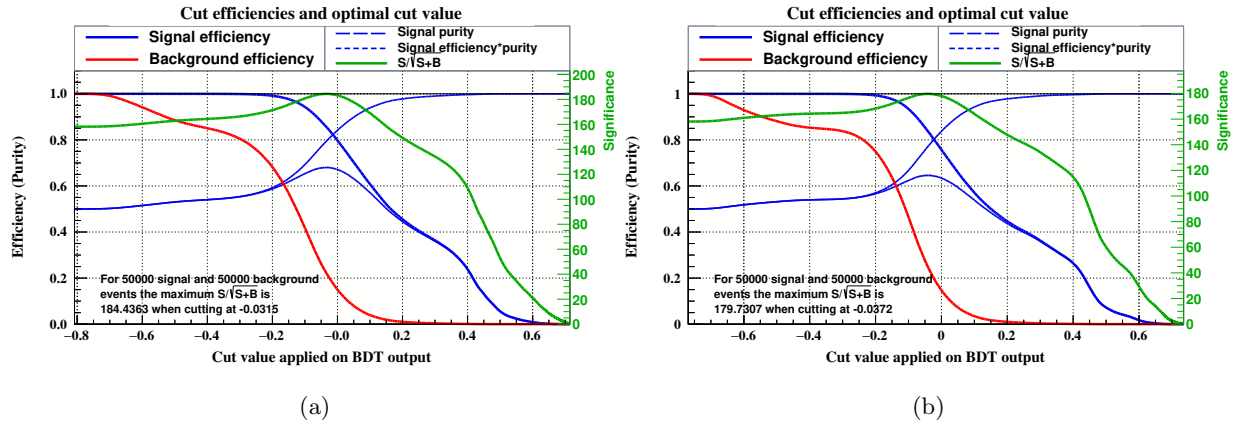


FIG. 12: BDT signal significance for fully hadronic on the left and semi-leptonic on the right respectively (with cuts).

The **Significance** of the signal process is used in high-energy physics (HEP) to quantify its separation. In the context of a third-generation scalar Leptoquark (involving hadronic mode), the likelihood classifier yields the highest signal significance as well as highest signal efficiency and background efficiency. This indicates that the classifier is successfully and accurately differentiating between the signal (instances of the third-generation scalar Leptoquark) and background (other events or particles). This demonstrates that the classifier is effectively detecting the intended signal

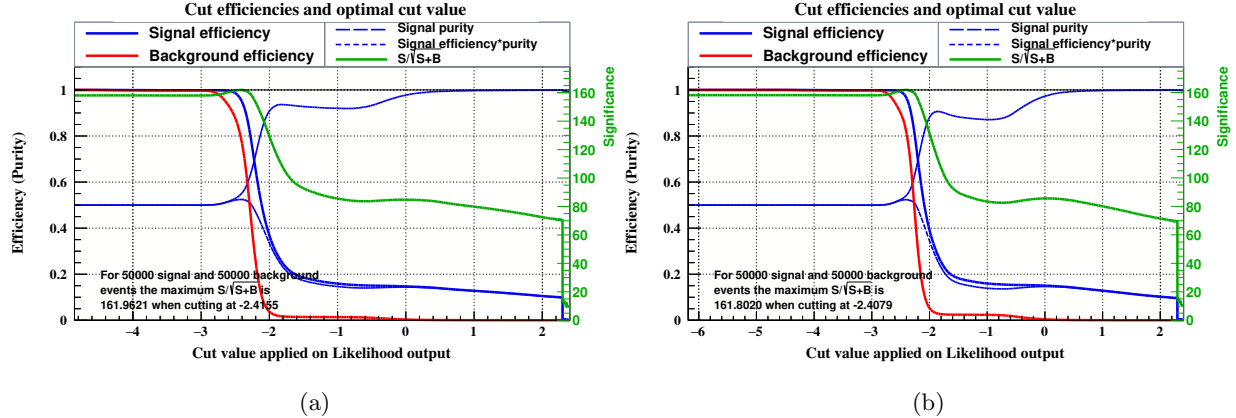


FIG. 13: Likelihood signal significance for fully hadronic on the left and semi-leptonic on the right respectively (with cuts).

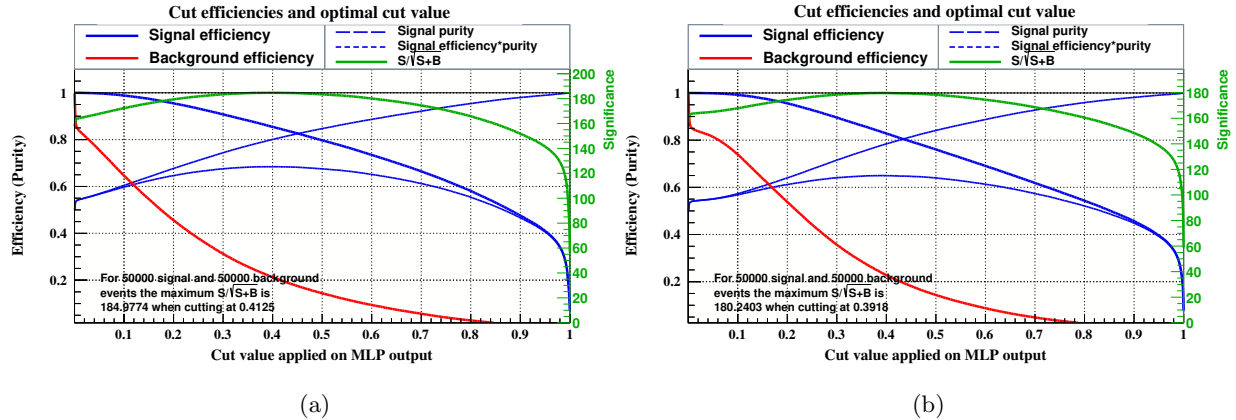


FIG. 14: MLP signal significance for fully hadronic on the left and semi-leptonic on the right respectively (with cuts).

while reducing background false positives. For instance, MLP classifier gives signal significance up to 184.98 with applying cuts. Similarly, the behavior for other classifiers can be seen from Table IVThe optimal-cuts, signal-background ratio, signal, and background efficiency for the number of signal and background events. Similarly for semi-leptonic decay mode MLP showing maximum value of signal significance with applying cuts. For MLP, signal significance is improved by applying cuts up to 180.24. While for BDT signal significance improved up to 179.73 with applying cuts Table VThe optimal-cuts, signal-background ratio, signal, and background efficiency for the number of signal and background events. This finding may suggest that the MLP design better captures the fundamental physics of the Leptoquark, which enables it to attain larger signal significance than other classifiers. The MLP's higher performance in this situation may be attributed in part to its flexibility in modeling

complicated events and its capacity to understand nuanced correlations within the data.

MVA Classifier	Optimal-Cut	$\frac{S}{\sqrt{S+B}}$	Sig-Eff	Bkg-Eff
Likelihood	-2.415	161.96	0.957	0.789
MLP	0.412	184.98	0.847	0.202
BDT	-0.031	184.43	0.852	0.215

TABLE IV: The optimal-cuts, signal-background ratio, signal, and background efficiency for the number of signal and background with applying cuts (fully hadronic).

MVA Classifier	Optimal-Cut	$\frac{S}{\sqrt{S+B}}$	Sig-Eff	Bkg-Eff
Likelihood	-2.407	161.80	0.968	0.823
MLP	0.391	180.24	0.833	0.236
BDT	-0.037	179.73	0.830	0.237

TABLE V: The optimal-cuts, signal-background ratio, signal, and background efficiency for the number of signal and background with applying cuts (semi-leptonic).

Table VI Comparison of Significance regarding MA5 and MVA table.6 shows a comparison of signal significance for Madanalysis5 (MA5) and Multivariate Analysis (MVA) at two different masses of leptoquarks. This shows that MVA gives higher values of signal significance as compared to MA5. Like for instance, at 500 GeV MA5 gives a significance of 17.59 while MVA gives 176.70 and 168.56 for fully hadronic and semi-leptonic modes respectively. Multiple factors may be taken into account concurrently by MVAs, improving the ability to distinguish between signal and background events. When working with intricate signal distributions or overlapping backgrounds, this

LQ Mass	MA5 Results	MVA Results (Fully Hadronic)	MVA Results
			(Semi-leptonic)
	$\frac{S}{\sqrt{S+B}}$	$\frac{S}{\sqrt{S+B}}$	$\frac{S}{\sqrt{S+B}}$
500 GeV	17.59	176.70	168.56
2 TeV	0.011	184.27	181.89

TABLE VI: Comparison of Significance regarding MA5 and MVA.

is quite helpful. Also, MVAs may be able to pick up on minute variations that straightforward cut-based techniques could miss by tailoring the selection criteria according to the properties of the signal and background distributions. In outcome, MVA outperforms cut-based analysis in this situation because it can efficiently use numerous variables, optimize selection criteria, minimize information loss, consider correlations, and remain robust under a variety of circumstances.

VII. CONCLUSION

In this work, we reported the results of leptoquark searches at the TeV scale using neural networks from various decay modes to explore the discovery potential of LQs, which are under investigation by the ATLAS and the CMS detectors of the LHC. In particular, the dominating decay of a scalar leptoquark into third-generation quarks and leptons in fully hadronic, as well as the semi-leptonic decay modes, were the main attention of research in this article. The final states were selected by well-defined cumulative cuts resulting from leptoquark pair generation at the $\sqrt{s} = 14 \text{ TeV}$ by selecting some appropriate benchmark points as mentioned in Table IIBenchmark scenarios for third generation scalar $LQ_{stable.2}$. We accounted mass Vs cross-section, energy Vs cross-section, λ Vs σ and λ Vs $\Gamma_{partial}$ in our work. In the next step, we performed the kinematical analysis in which we reconstructed the invariant mass of leptoquarks for different quarks flavor, along with transverse momentum (p_t^j), pseudorapidity (η) at different integrated luminosity. To achieve strong distinguishing strength against background processes, neural networks were trained for a variety of signal possibilities. The classification was accomplished via MVA by creating a classifier output using the input variables (referred to as observables). Signal events were represented in this output by values close to 1, whereas background events were represented by values close to 0. We observed that the best classifiers were Multilayer Perceptron (MLP), Likelihood, Boosted/Bagged Decision Trees (BDTs), which improved the signal significance when cuts were implemented. For the hadronic decay mode, the signal efficiency was improved for the MLP, Likelihood, and BDT having values of 0.847, 0.96, and 0.85, respectively by applying cuts. For the semi-leptonic decay mode, these classifiers predicted the signal efficiency of 0.833, 0.968, and 0.830, respectively with such cuts. The best classifier for third-generation sLQ in terms of signal significance was found **MLP** for both decay modes. **MLP** also indicated the higher **ROC** curve for both of the decay mode. Upon comparison with the MA5, MVA provided a more comprehensive method for separating signals from background events. This result opened up new avenues for investigating basic particles and their interactions. Further, it emphasizes how

crucial it is to use sophisticated analytic tools to increase the sensitivity and accuracy of particle physics investigations.

VIII. ACKNOWLEDGEMENTS

We gratefully acknowledge support from the Simons Foundation and member institutions. The current submitted version of the manuscript is available on the arXiv pre-prints home page.

IX. STATEMENTS AND DECLARATIONS

Funding

The authors declare that no funds, grants, or other support were received during the preparation of this manuscript.

Competing Interests

The authors have no relevant financial or non-financial interests to disclose.

Availability of data and materials

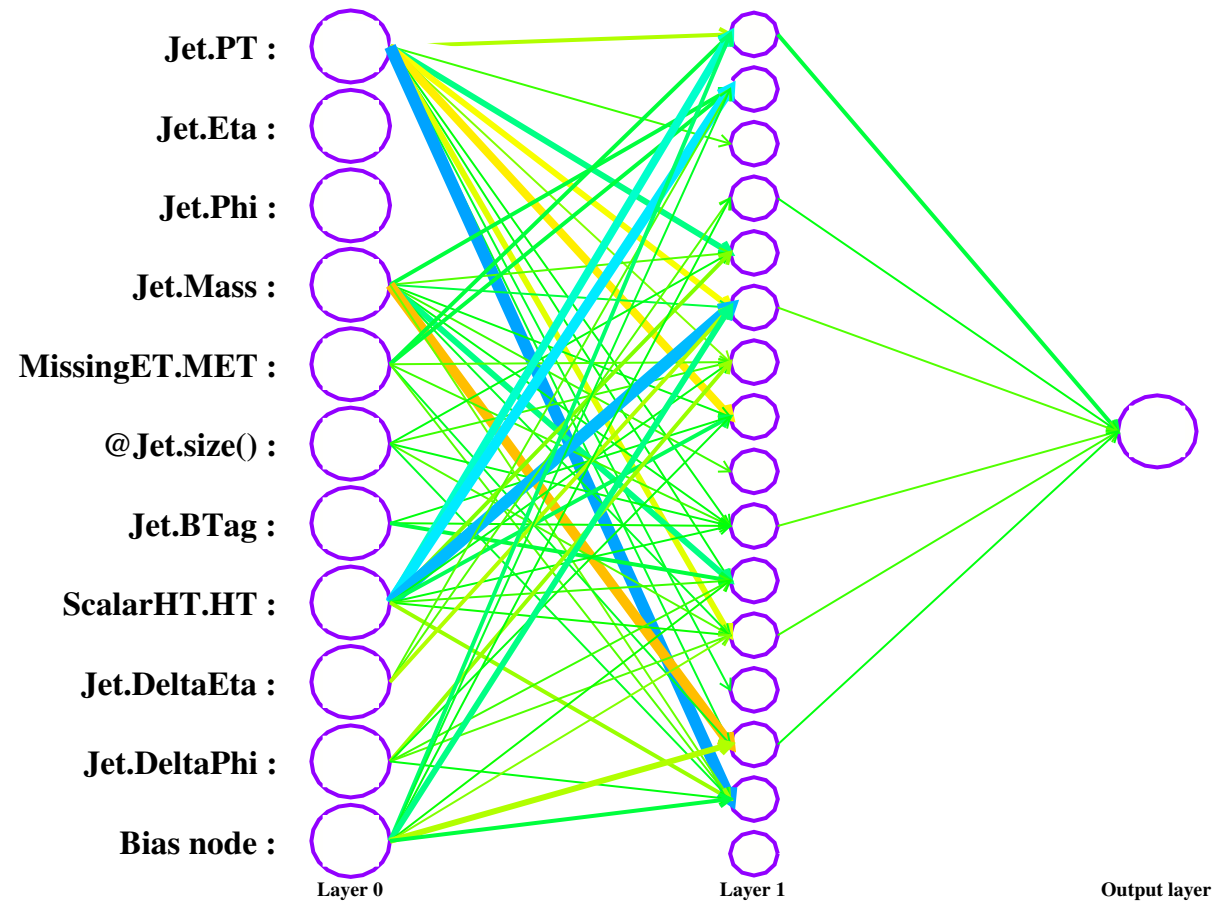
Data sharing is not applicable to this article as no datasets were generated or analyzed during the current study.

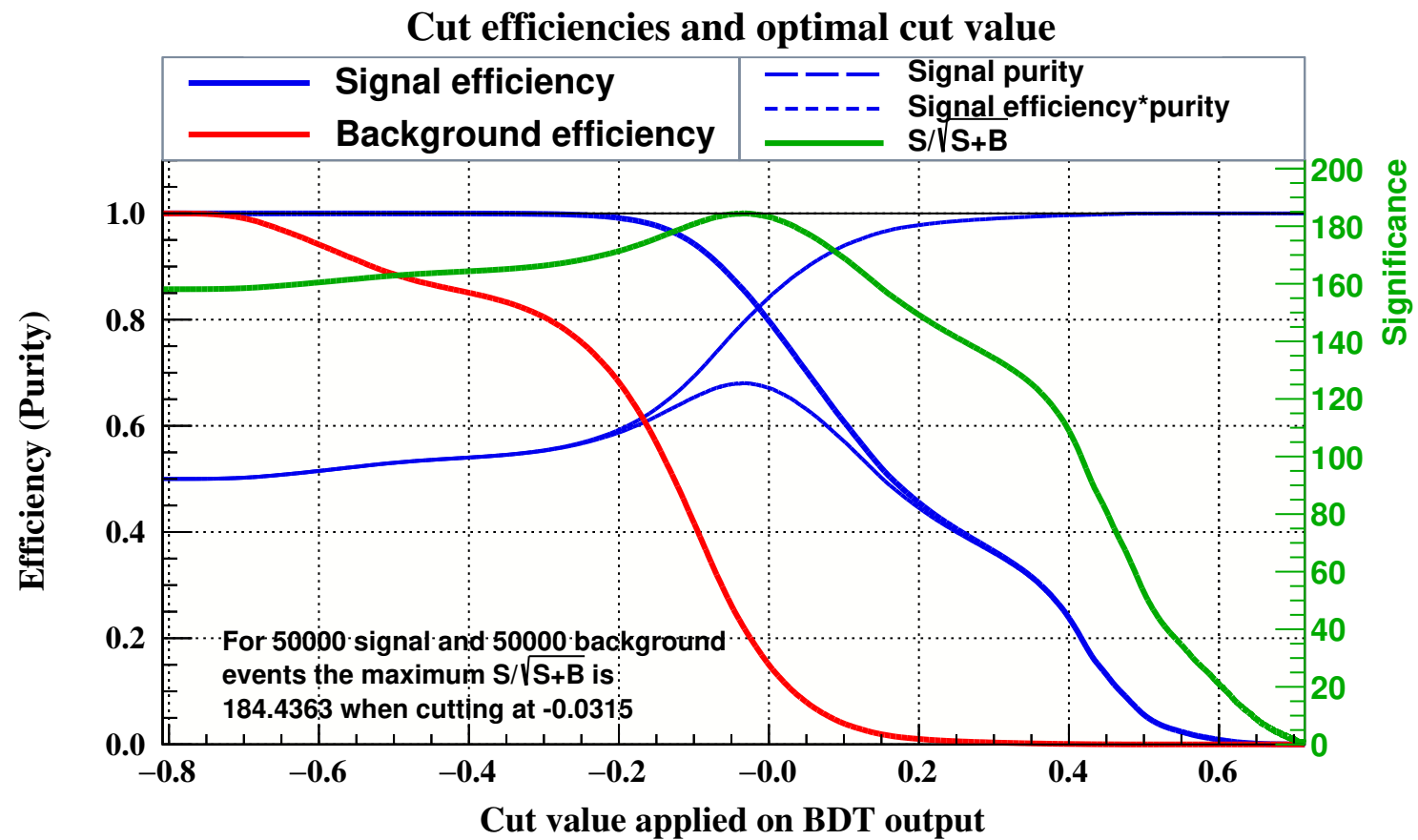
- [1] J. Lees, V. Poireau, V. Tisserand, J. G. Tico, E. Grauges, A. Palano, G. Eigen, B. Stugu, D. N. Brown, L. Kerth, *et al.*, “Evidence for an excess of $\bar{B} \rightarrow d^{(*)}\tau^{(-)}\bar{\nu}\tau$ decays,” *Physical review letters*, vol. 109, no. 10, p. 101802, 2012.
- [2] B. Bhattacharya, A. Datta, D. London, and S. Shivashankara, “Simultaneous explanation of the rk and r (d (*)) puzzles,” *Physics Letters B*, vol. 742, pp. 370–374, 2015.
- [3] J. C. Pati and A. Salam, “Lepton number as the fourth” color”,,” *Physical Review D*, vol. 10, no. 1, p. 275, 1974.
- [4] H. Georgi and S. L. Glashow, “Unity of all elementary-particle forces,” *Physical Review Letters*, vol. 32, no. 8, p. 438, 1974.
- [5] S. Dimopoulos and L. Susskind, “Mass without scalars,” *Nuclear Physics B*, vol. 155, no. 1, pp. 237–252, 1979.
- [6] S. Dimopoulos, “Technicoloured signatures,” *Nuclear Physics B*, vol. 168, no. 1, pp. 69–92, 1980.

- [7] E. Eichten and K. Lane, “Dynamical breaking of weak interaction symmetries,” *Physics Letters B*, vol. 90, no. 1-2, pp. 125–130, 1980.
- [8] V. Angelopoulos, J. Ellis, H. Kowalski, D. V. Nanopoulos, N. Tracas, and F. Zwirner, “Search for new quarks suggested by the superstring,” *Nuclear Physics B*, vol. 292, pp. 59–92, 1987.
- [9] W. Buchmüller and D. Wyler, “Constraints on su (5)-type leptoquarks,” *Physics Letters B*, vol. 177, no. 3-4, pp. 377–382, 1986.
- [10] R. Iuppa, A. Di Luca, C. Atlas, *et al.*, “Searches for third-generation scalar leptoquarks in $\sqrt{s} = 13$ tev pp collisions with the atlas detector,” *INTERNATIONAL JOURNAL OF HIGH ENERGY PHYSICS*, vol. 2019, no. 6, 2019.
- [11] C. Lo, C. PENG, K. TAM, L. Pizzimento, A. collaboration, *et al.*, “Search for pair production of third-generation scalar leptoquarks decaying into a top quark and a τ lepton in pp collisions at $\sqrt{s} = 13$ tev with the atlas detector,” *Journal of High Energy Physics*, 2021.
- [12] A. M. Sirunyan, A. Tumasyan, W. Adam, F. Ambrogi, E. Asilar, T. Bergauer, J. Brandstetter, M. Dragicevic, J. Erö, A. E. Del Valle, *et al.*, “Search for pair production of first-generation scalar leptoquarks at $\sqrt{s} = 13$ tev,” *Physical Review D*, vol. 99, no. 5, p. 052002, 2019.
- [13] G. Aad, B. Abbott, D. C. Abbott, A. A. Abud, K. Abeling, D. K. Abhayasinghe, S. H. Abidi, O. AbouZeid, N. L. Abraham, H. Abramowicz, *et al.*, “Search for a scalar partner of the top quark in the all-hadronic $t\bar{t}$ plus missing transverse momentum final state at $\sqrt{s} = 13$ tev with the atlas detector,” *The European Physical Journal C*, vol. 80, no. 8, p. 737, 2020.
- [14] G. Aad, B. Abbott, D. C. Abbott, A. A. Abud, K. Abeling, D. K. Abhayasinghe, S. H. Abidi, O. AbouZeid, H. Abramowicz, H. Abreu, *et al.*, “Search for new phenomena in p p collisions in final states with tau leptons, b-jets, and missing transverse momentum with the atlas detector,” *Physical Review D*, vol. 104, no. 11, p. 112005, 2021.
- [15] P. Bandyopadhyay and R. Mandal, “Vacuum stability in an extended standard model with a leptoquark,” *Physical Review D*, vol. 95, no. 3, p. 035007, 2017.
- [16] C. collaboration *et al.*, “Search for pair production of second-generation leptoquarks at $\sqrt{s} = 13$ tev,” *arXiv preprint arXiv:1808.05082*, 2018.
- [17] A. Collaboration *et al.*, “Search for pair production of scalar leptoquarks decaying into first- or second-generation leptons and top quarks in proton-proton collisions at $\sqrt{s} = 13$ tev with the atlas detector,” *arXiv preprint arXiv:2010.02098*, 2020.
- [18] C. collaboration *et al.*, “Search for singly and pair-produced leptoquarks coupling to third-generation fermions in proton-proton collisions at $\sqrt{s} = 13$ tev,” *arXiv preprint arXiv:2012.04178*, 2020.
- [19] G. Aad, B. Abbott, K. Abeling, S. Abidi, A. Aboulhorma, H. Abramowicz, H. Abreu, Y. Abulaiti, A. A. Hoffman, B. Acharya, *et al.*, “Search for pair production of third-generation

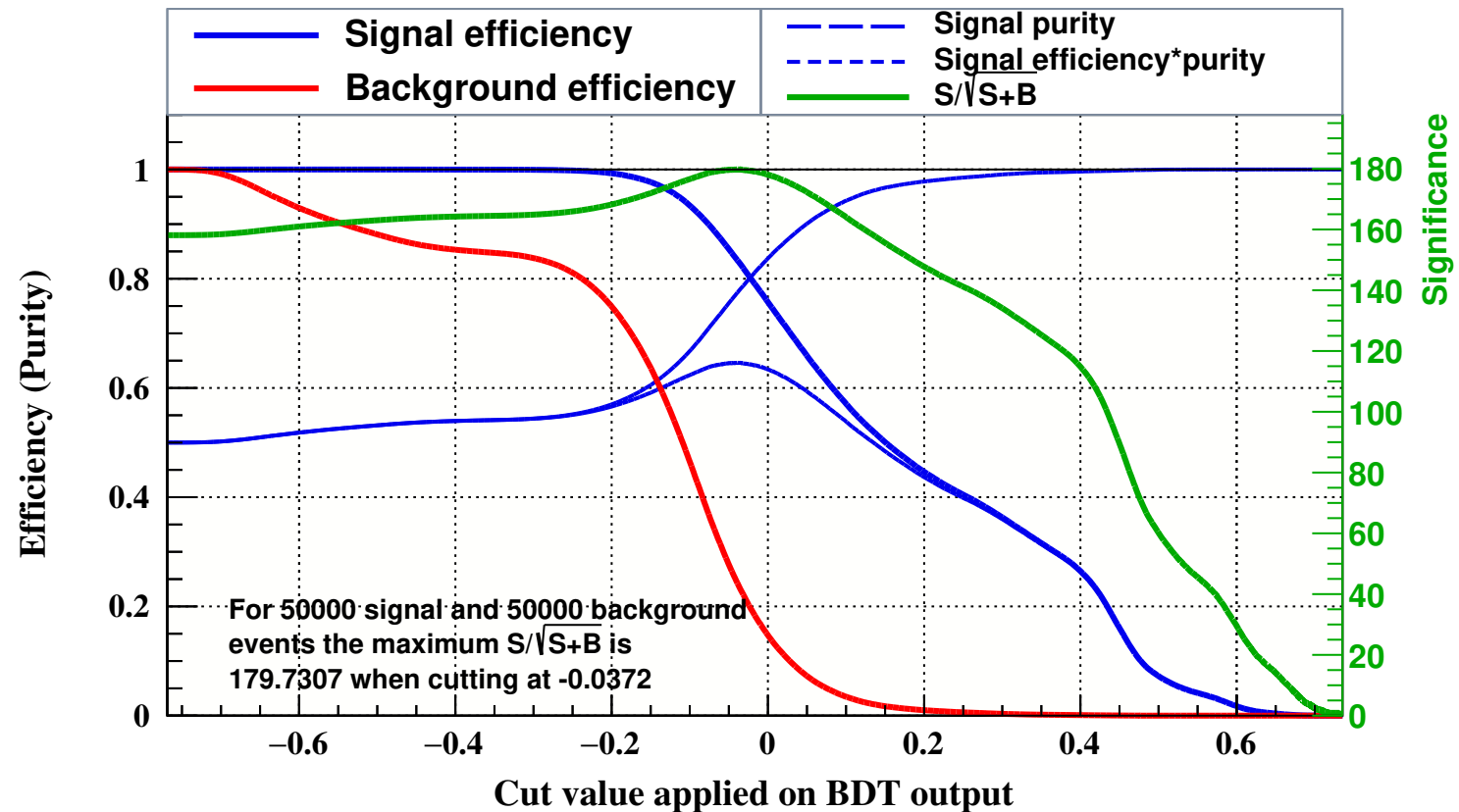
leptoquarks decaying into a bottom quark and a τ -lepton with the atlas detector,” *The European Physical Journal C*, vol. 83, no. 11, p. 1075, 2023.

- [20] M. Hirsch, H. Klapdor-Kleingrothaus, and S. Kovalenko, “New leptoquark mechanism of neutrinoless double β decay,” *Physical Review D*, vol. 54, no. 7, p. R4207, 1996.
- [21] A. Davies and X.-G. He, “Tree-level scalar-fermion interactions consistent with the symmetries of the standard model,” *Physical Review D*, vol. 43, no. 1, p. 225, 1991.
- [22] S. Maes, “A bold prediction on the muon anomalous magnetic moment, and expected resulted to be published on april 7, 2021 by the fermilab muon g-2, and its explanation,” 2022.
- [23] A. Belyaev, C. Leroy, R. Mehdiyev, and A. Pukhov, “Leptoquark single and pair production at lhc with calchep/comphew in the complete model,” *Journal of High Energy Physics*, vol. 2005, no. 09, p. 005, 2005.
- [24] J. Hewett and S. Pakvasa, “Scalar-leptoquark production at hadron colliders,” *Physical Review D*, vol. 37, no. 11, p. 3165, 1988.
- [25] R. Brun and F. Rademakers, “Root—an object oriented data analysis framework,” *Nuclear instruments and methods in physics research section A: accelerators, spectrometers, detectors and associated equipment*, vol. 389, no. 1-2, pp. 81–86, 1997.
- [26] A. Hoecker, P. Speckmayer, J. Stelzer, J. Therhaag, E. von Toerne, H. Voss, M. Backes, T. Carli, O. Cohen, A. Christov, *et al.*, “Tmva-toolkit for multivariate data analysis,” *arXiv preprint physics/0703039*, 2007.
- [27] R. Y. Choi, A. S. Coyner, J. Kalpathy-Cramer, M. F. Chiang, and J. P. Campbell, “Introduction to machine learning, neural networks, and deep learning,” *Translational vision science & technology*, vol. 9, no. 2, pp. 14–14, 2020.

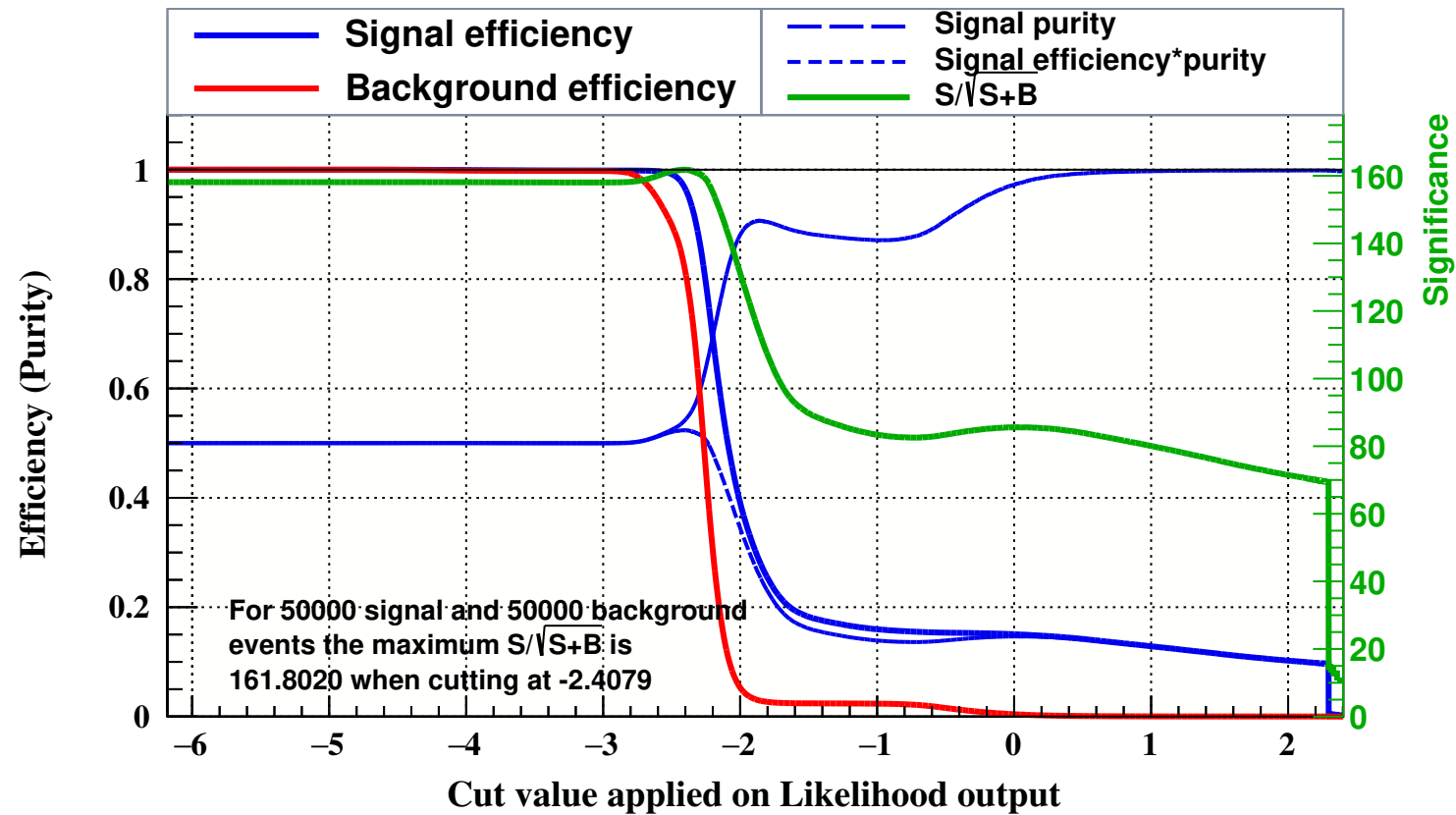




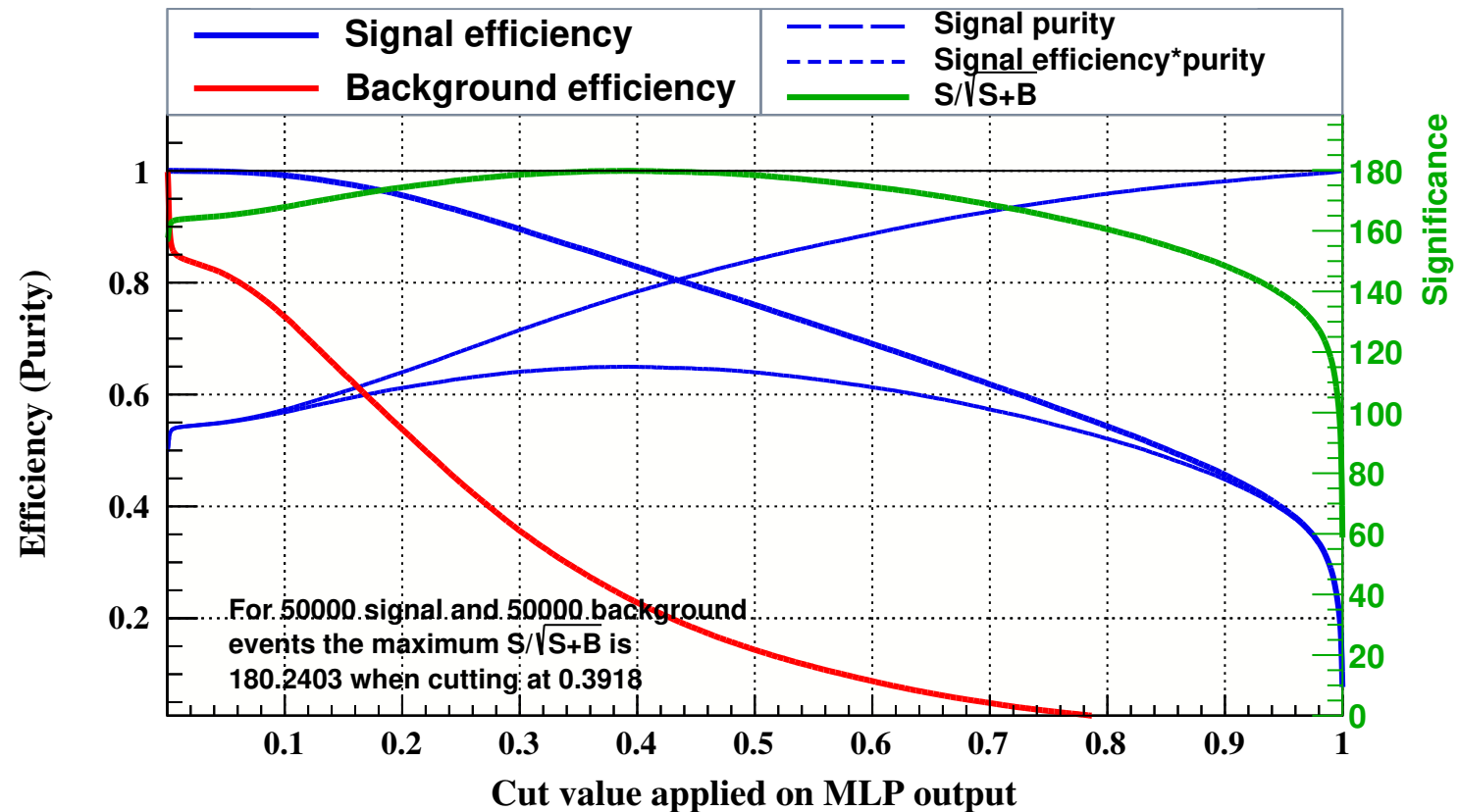
Cut efficiencies and optimal cut value

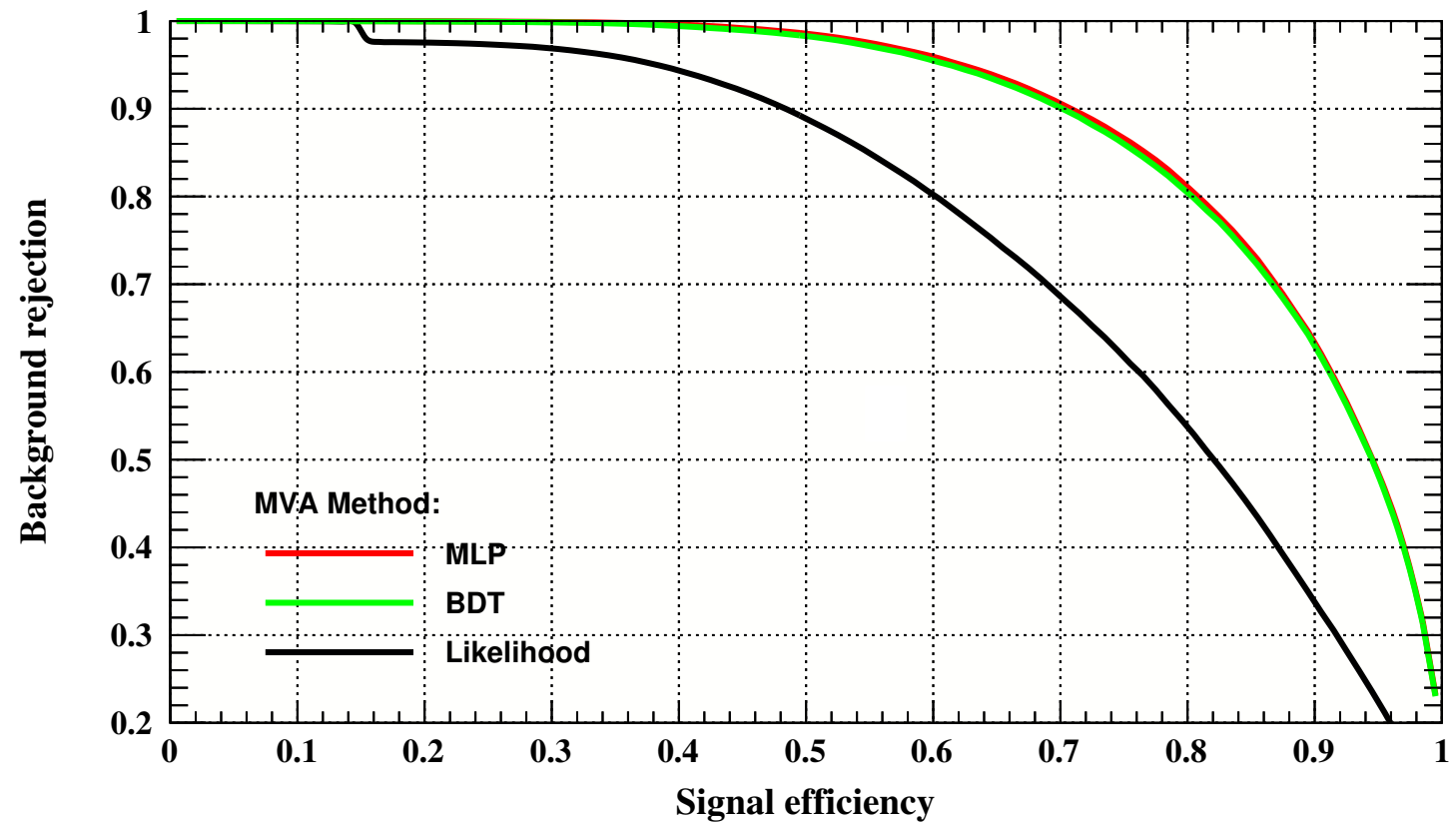


Cut efficiencies and optimal cut value

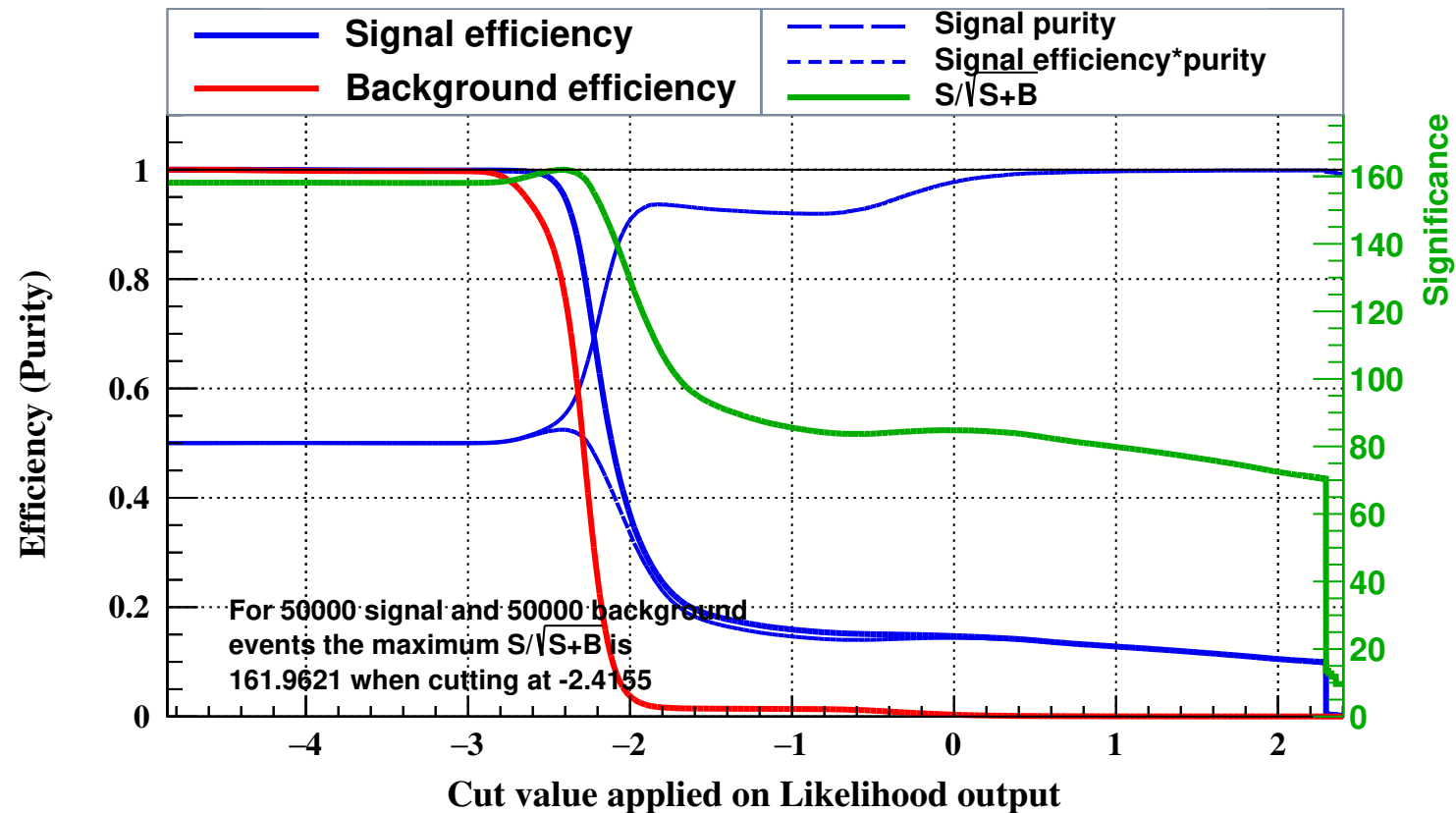


Cut efficiencies and optimal cut value

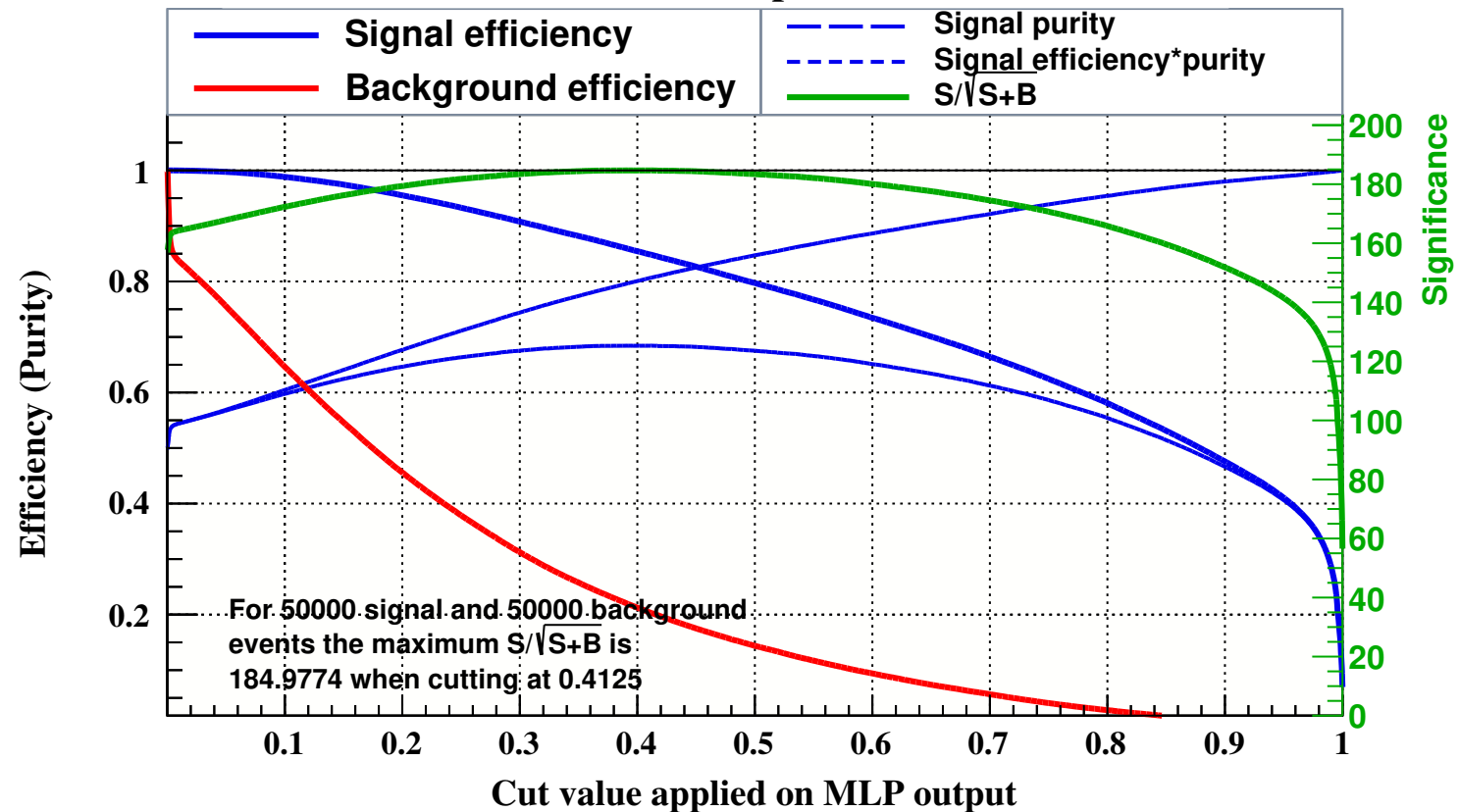


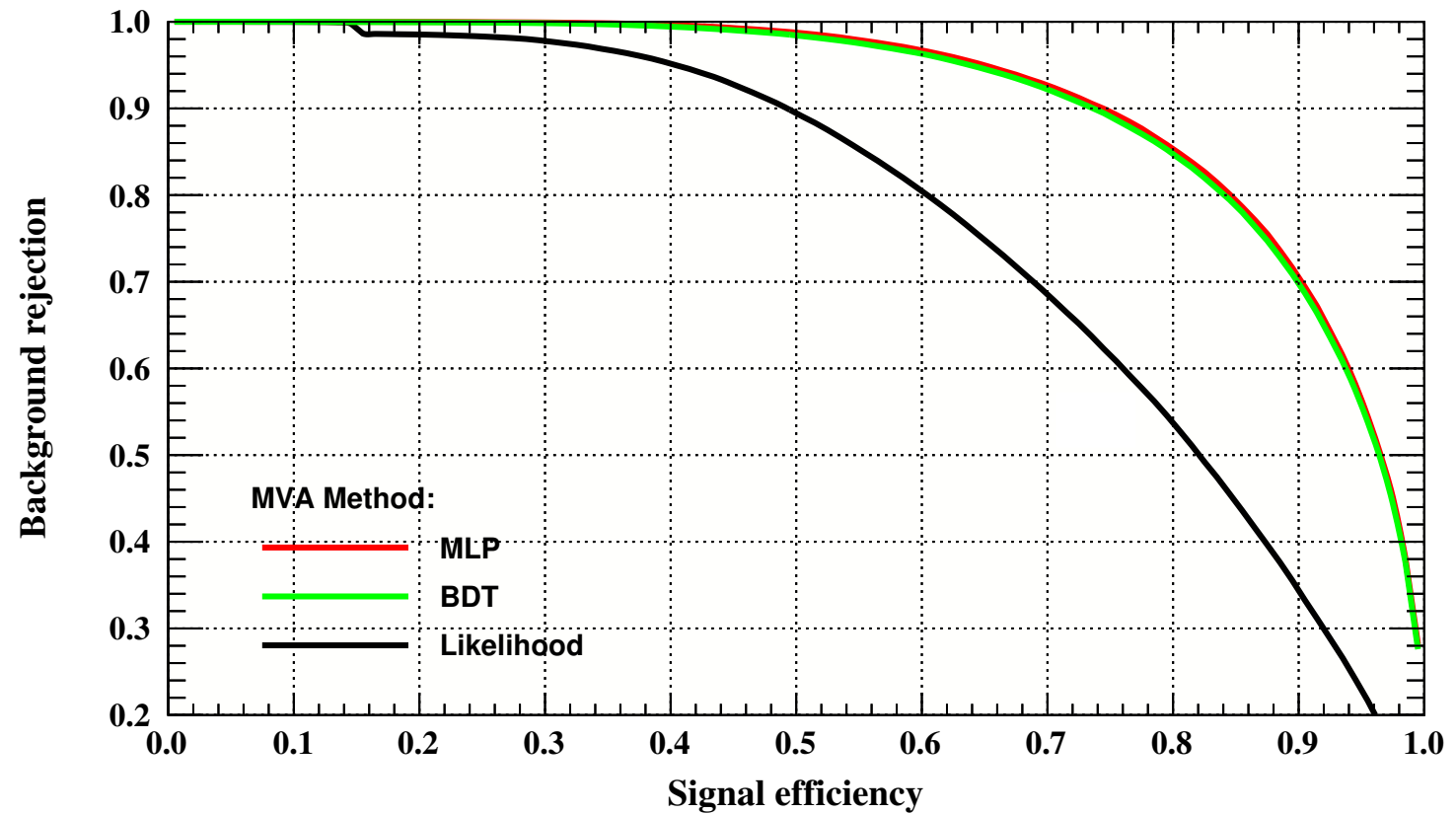


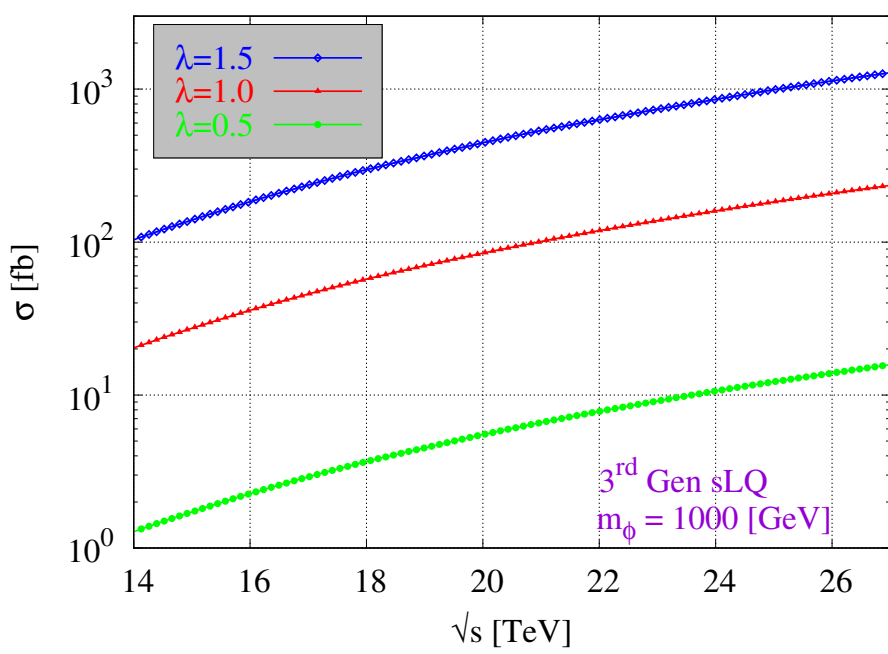
Cut efficiencies and optimal cut value

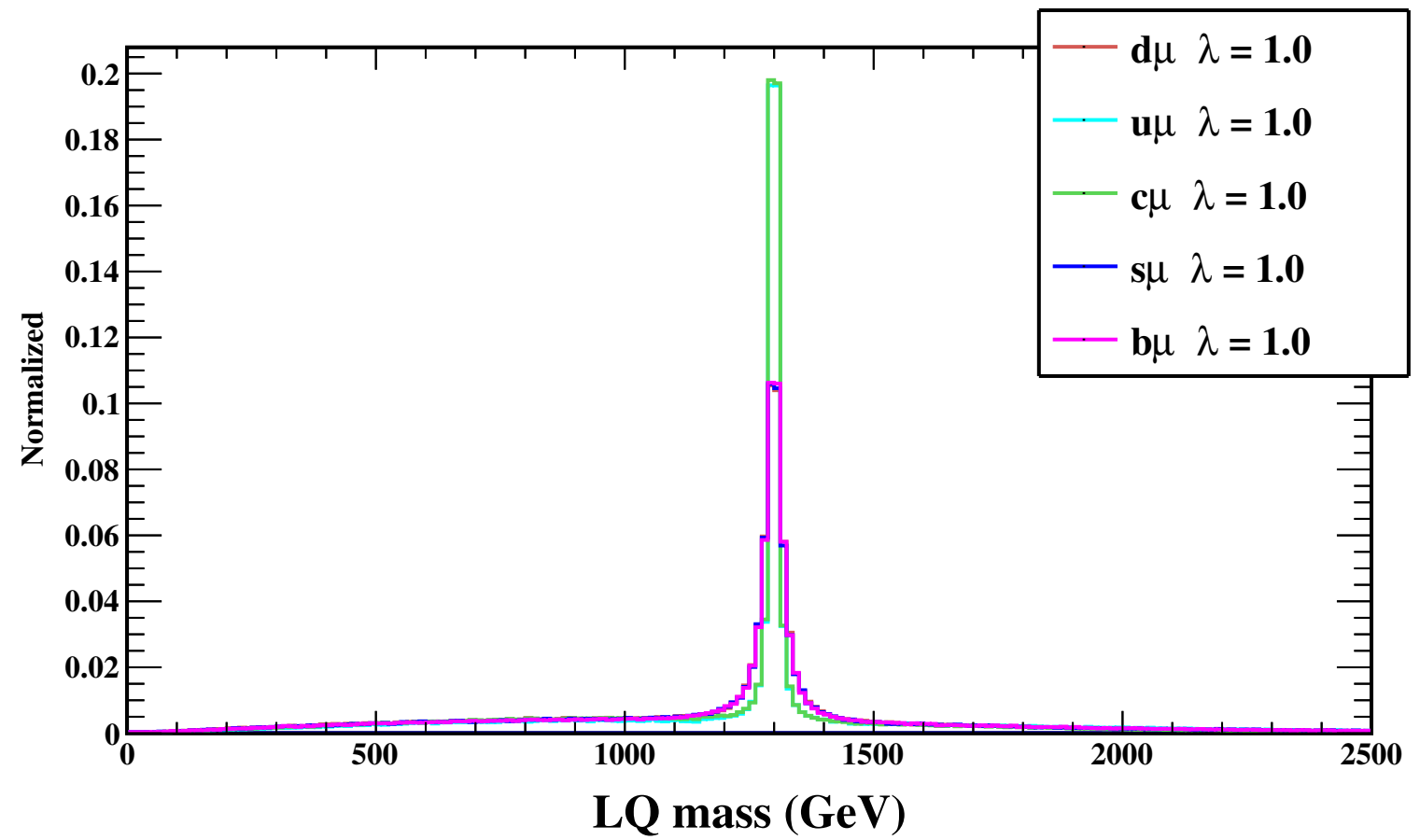


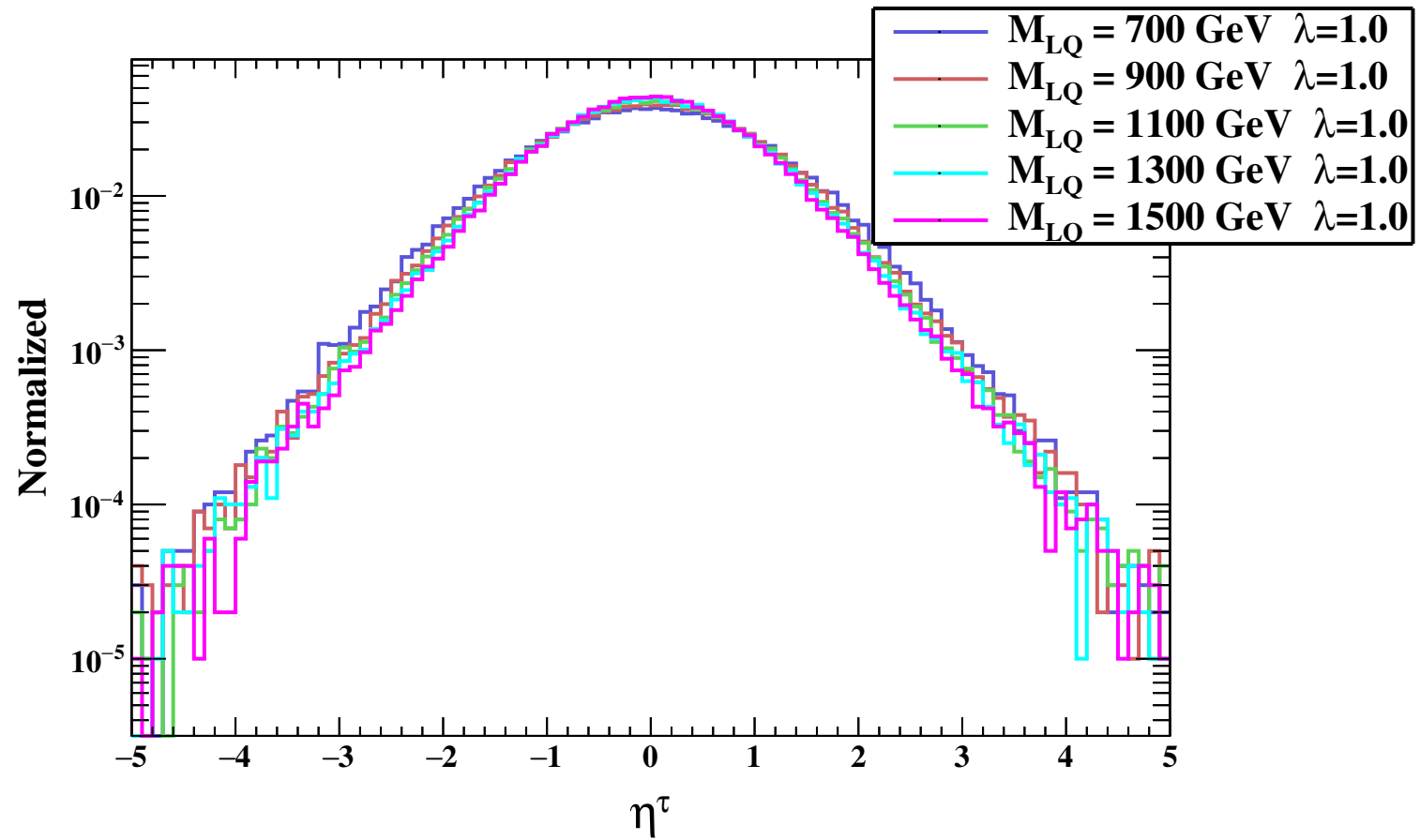
Cut efficiencies and optimal cut value

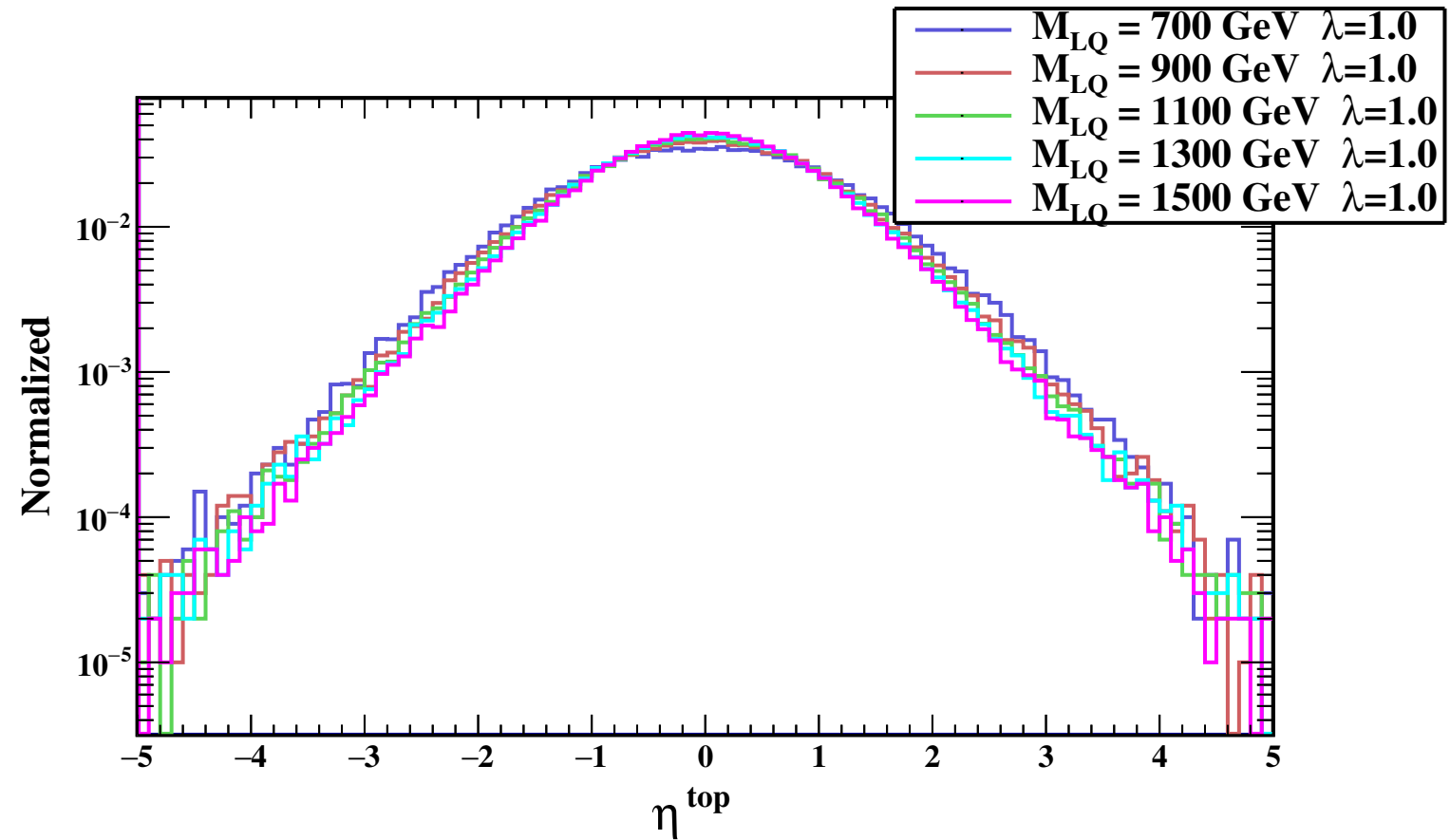


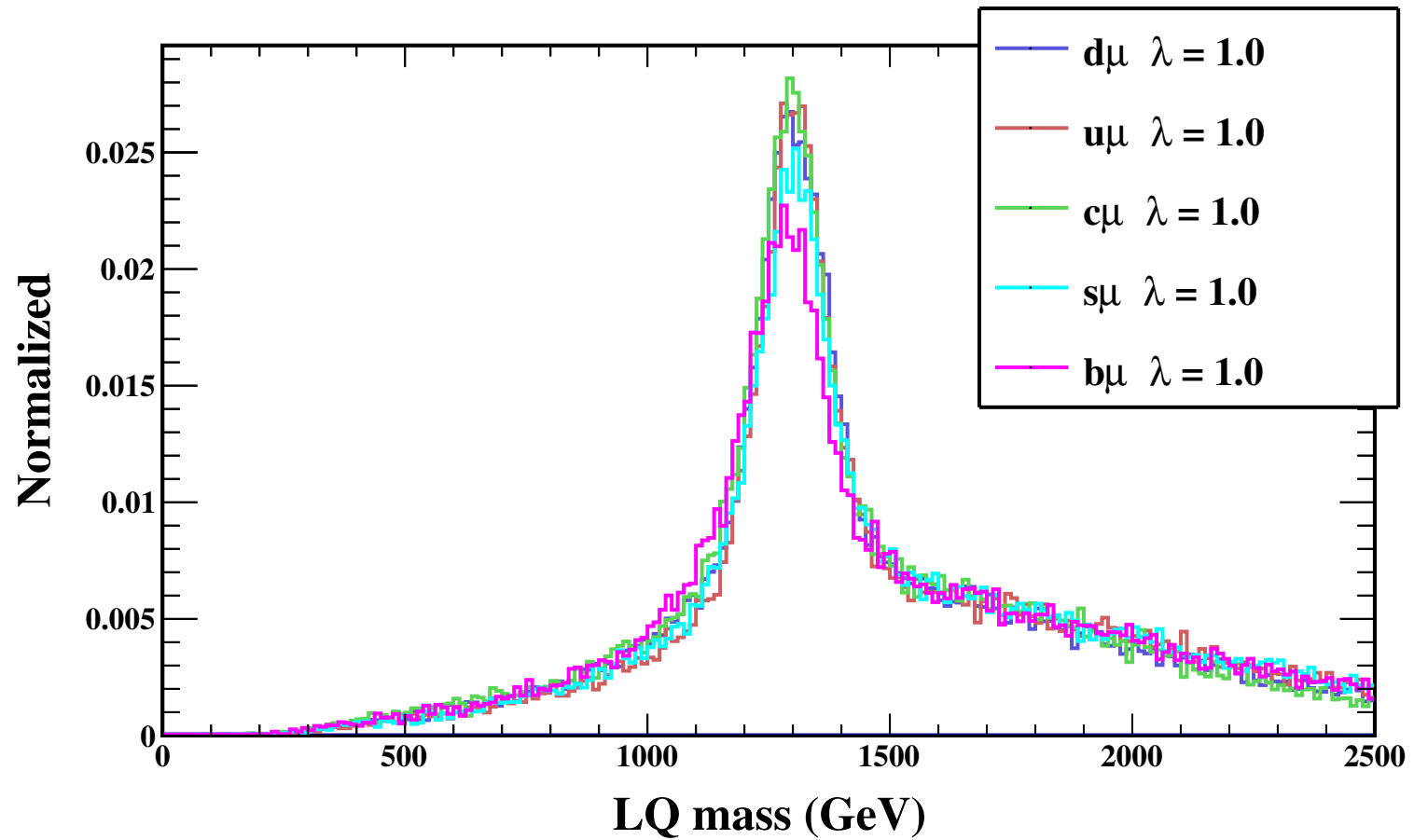


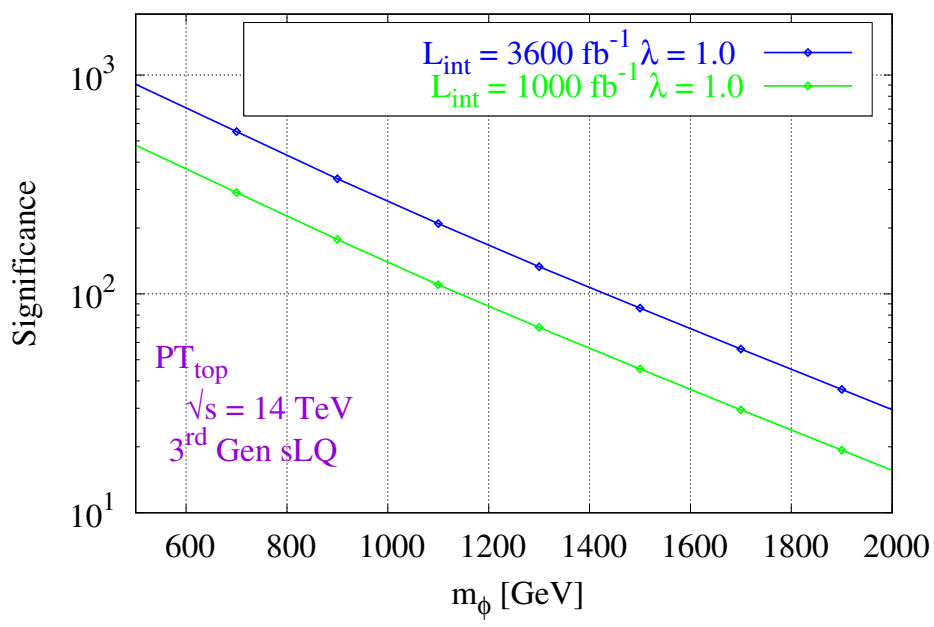


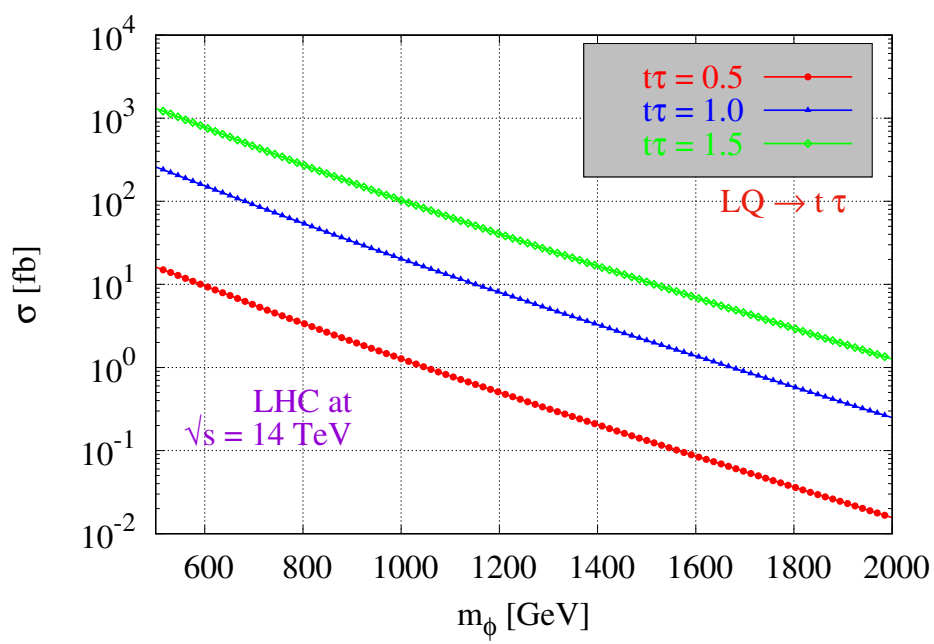












Significance

